UNIVERSIDADE DA BEIRA INTERIOR

ENGENHARIA

# Development and Testing of a Variable-Spam Morphing Wing

## João Miguel Inácio Felício

Dissertação para obtenção do Grau de Mestre em

## Engenharia Aeronáutica

(2º ciclo de estudos)

Orientador: Prof. Doutor Pedro Gamboa

**Covilhã, Outubro de 2010**

# Abstract

Motivation for the work.

The present work focuses on the development and validation of a variable-span morphing wing (VSW) to be fitted to a mini UAV. An electro-mechanical actuation mechanism is developed using a simple rack and pinion system. The wing model is designed with the help of graphical CAD/CAE tools and then a full scale model is built for bench testing the strength, power consumption, deployment time and efficiency. The concepts used on the morphing wing for both fixed and moving wing parts are considered simple and effective. Construction methods and materials were evaluated in order to obtain a system as reliable as possible. Still, in future work the VSW structure can be improved by changing some interface components to achieve a smoother deployment. Also, some work is planned on the design optimization code: implementation of a coupled aero-structural analysis model for simultaneous aerodynamic and structural design optimization problems.

Main results: deployment times; efficiency.

# Resumo

O presente trabalho apresenta o desenvolvimento e ensaio de uma asa de envergadura variável actuada por um sistema electromecânico simples para aplicação no UAV "Olharapo". Um mecanismo de accionamento electromecânico é desenvolvido com base num sistema de cremalheira e pinhão. O modelo da asa é projectado com a ajuda de ferramentas gráficas CAD / CAE e, em posteriormente, é construído um modelo em escala para ensaios quanto a resistência, consumo de energia, tempo de extensão/retracção e eficiência. Os conceitos utilizados na asa morphing para ambas as partes, fixas e móveis, da asa são consideradas simples e eficazes. Foram avaliados métodos e materiais de construção no intuito de obter um sistema mais fiável e eficaz. Ainda assim, em trabalhos futuros a estrutura VSW pode ser melhorada alterando alguns componentes de interface para conseguir uma actuação mais suave e eficaz. Além disso, é previsto no código de optimização de envergadura capaz de controlar esta em função da velocidade.

# Acknowledgments

I would like to thank Dr. Pedro Gamboa for his continuous support and motivation. Without his guidance this project would not have been possible.

Also, I want to thank my parents for their strength in believing me in this chapter of my life.

Finally, I want to thank to Marta for her indispensable help, support and understanding.

# List of Figures

# List of Tables

# Nomenclature

b            Wng Spam

$C_D$         Drag Coefficient

$C_l$          Airfoil Coefficient

IFW       Inner Fixed Wing

$L$            Lift

$L/D$      Lift to Drag Ratio

UAV      Unmanned Aerial Vehicle

VSW      Variable Spam Wing

# Index

# Chapter 1

## Introduction

The yearning for a flight as efficient, noiseless and reliable as birds' still is a major intent for manhood. Even a century over achieving his first flight, followed by the supersonic speeds and space exploration in flying devices, Man remains highly ambitious as far as trying to mimic Nature. The capability of birds, in altering its flight's features according to velocity, and so increasing its flight envelope, became one of the most relevant differences comparing to aircraft.
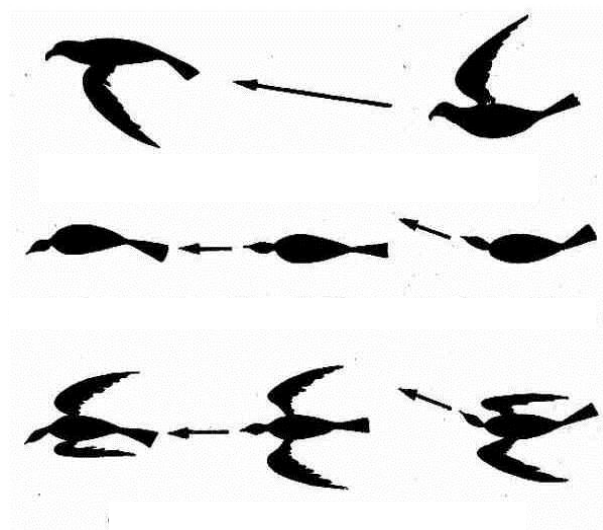
Figure 1.1 – Different flight configurations of a bird. [1]

Along the years, the need for energy efficiency played a significant role in the optimization of existing devices, aircraft included. That improvement was based on using lightweight materials, resourceful propulsive systems and also high-lift devices such as flaps and slats. Nowadays, the development of new materials and technologies allows engineers to overcome their own limits. Therefore, morphing wings became of higher interest over the past years requiring further studies and experimental projects.

---

[1] From, http://www.portalsaofrancisco.com.br/alfa/classe-aves/voo-das-aves-2.php

Morphing is a relatively recent concept, although relevant technology has been used since the first Wright Brother's flight, in which the wing's torsion controlled the roll. Other classic examples are the F-111, F-14 and B-1 aircraft (figure 1.2) whose swept wings were adapted according to speed.
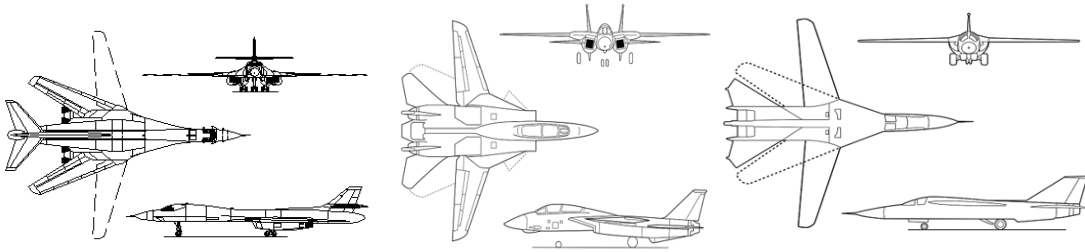


Figure 1.2 – B-1, F14 and F-111 aircrafts images. [2]

As time goes by, a completely adaptable aircraft becomes more and more feasible. The benefits of this technology can be quite extensive. Suppose a multifunctional Unmanned Aerial Vehicle (UAV) flying in a long range configuration, when facing an obstacle, such as enemy aircraft or anti-aerial batteries, it alters its features improving maneuverability in order to escape.

In this work, a telescopic wing able to modify its wingspan during flight was built and tested. The advantages include reduction of drag and enhanced flight envelope: range, cruise speed, among others.

## 1.1. State of the art

### 1.1.1. Akaflieg FS-29

It was in June 15th of 1975 when the first and only manned sailplane (Fig. 1.4) fitted with a telescopic wing took its first flight. Akademische Fliegergruppe Stuttgart created this aircraft which is capable of flying slowly, being elevated in a thermal column and, when achieving its intended altitude, retracts its wings and travels large distances in a higher cruise speed.

The actuation mechanism is controlled manually by the pilot. Due to high construction costs as well as its complexity and necessity of pilot's experience, this sailplane remained as a means of research. Currently, it can be found at the Deutsches Museum. The sailplane technical specifications are presented in Table 1.1.

---

[2] From, http://www.flightglobal.com
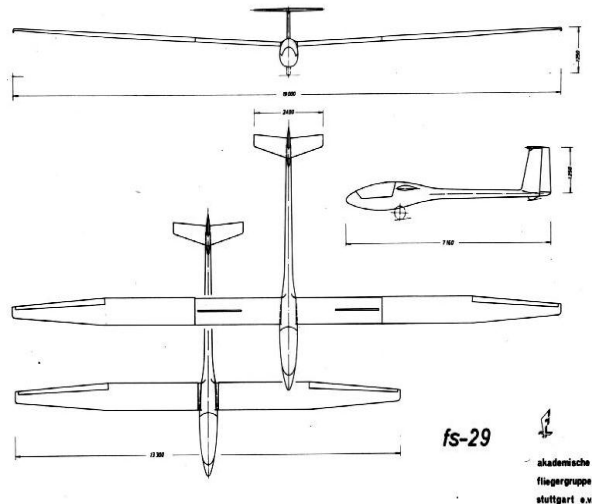
Figure 1.4 – Akaflieg FS-29 blueprint. [3]

| | |
|---|---|
| Span | 13.30 m to 19.00 (telescopic wing) |
| Area | 8.56 m$^2$ to 12.65 m$^2$ |
| Aspect ratio | 20.7 to 28.5 |
| Airfoil | FX 73-170 |
| Empty weight | 365 kg |
| Gross weight | 450 kg |
| Wing loading | 52.6 kg/m$^2$ |
| L/D max. | 44 at 98 Km/h |
| Minimum sink rate | 0.56 m/s at 81 Km/h |

Table 1.1 – FS-29 specifications. [3]

## 1.1.2. Telescopic spars

Several studies in morphing wing concepts were developed by Blondeau et al. from the University of Maryland over the past years [1,2,3 and 4]The research was based on the use of pneumatic telescopic spars. The key element of the project was the fact that the pressurized telescopic spar could undergo large-scale spanwise changes using telescopic skins so that the spanwise airfoil geometry could be preserved as well as the compactation and deployment of the wing.

---

[3] From, http://www.uni-stuttgart.de/akaflieg/

It is well known that range and endurance are strongly dependent on $C_l/C_D$ and $C_l^{3/2}/C_D$, respectively, which, in turn, depend on the wing aspect ratio. So, he concluded that, by tailoring the wing geometry it is possible to adapt the lift and drag to a diversity of operations.

The pneumatic system, compared to a lead-screw mechanism controlling the extension and retraction of the wings, appeared to be less expensive and more attractive presenting the following advantages: light weight, compactness, compliance tailoring and minimal moving parts. It was constituted by an aluminum telescopic inflatable spar with three elements and its extension/retraction control mechanism, length sensors, ribs fixed at the end of each section of the spar, fiberglass telescopic skins and a pressurized air source. The change of the pressure in the chambers was used to control the extension or retraction of the telescopic spar. In order to have a continuous sensing device to control deployment length, Blondeau used a system of rack and pinion mounted on a potentiometer to sense the displacement. Both structural and dynamic performances were taken into account, leading to the conclusion that the maximum tolerable wing loading was 1532 Pa, and that the spar could fully extend or retract in about 0,55 and 0,75 seconds, respectively, with a pressure input of $6x10^5$ Pa..

The theoretical aerodynamic performance was also estimated and compared with the final wind tunnel results coming from the tests of a smaller prototype of the spar, which was built to fit in the wind tunnel. Two tests were done: (a) with the wing fully retracted (wingspan of 7 in), and another (b) with the wing completely extended (wingspan of 15 in). Comparing to a fixed wing with the same dimensions, test (a) revealed that the telescopic wing presented a higher lift coefficient, a lower drag for all angles of attack and also a higher lift-to-drag ratio of approximately 15% except for near stall conditions. Such improvement can be explained by less friction drag and a more flexible wing tip. As for test (b), the results were quite unfavorable for the telescopic wing and the 25% lower lift-to-drag ratio remained partially unexplained. Significant wing twist at angles of attack greater than 5 degrees could be pointed as a cause to those results.

In a project developed in 2004, Blondeau [2], in order to solve the uncontrolled vibration and twisting exhibited of the earlier wing, used two pneumatic telescopic actuators positioned side by side. Keeping similarities with the previous design, the construction, the air pressurized system and valves suffered some minor alterations in the extension/retraction system scheme. Wind tunnel testing for three different Reynolds numbers, four different spans, and angle of attack ranging from 0 to 24 degrees showed that the fixed wing still exhibited higher lift and lower drag comparing to the telescopic wing. The flexibility of the wing was referred as the cause for that, since the increase of the angle of attack was accompanied by a lower airfoil surface susceptible to be deformed by pressure, although that situation was not consistently observed. The reduction in aerodynamic performance can also be attributed to the roughness of the skin and possibly the seams of the wing sections.

By their third project, in 2007, Blondeau and Pines [3] covered the seams with a thin aluminum foil tape to seal them in a static study. There was also added some friction tape in an area where the boundary layer should be and remained attached. Then, they evaluated its impact on the aerodynamic performance. The function of the friction tape was to ease the deployment/retraction on the telescopic wing. The same pattern of the friction tape was used in the solid wing so that results could be compared. These tests were also performed in its absence. The results were conclusive: the lift was enhanced consistently with covered seams, and was even higher when coming closer to stall speeds leading to an improved L/D at almost all speeds, comparing to the telescopic wing with uncovered seams. Nonetheless, as aerodynamic performance was concerned the friction tape showed no effect.

A morphing wing concept for an experimental UAV was presented by Gamboa et al [10]. A set of optimal wing shapes for minimum drag for a range of flight speeds was intended to be obtained by using a multidisciplinary design optimization tool, so that the vehicle's performance was improved. The aerodynamic shape optimization code used a 2-dimensional panel method formulation coupled with a non-linear lifting-line algorithm and a sequential quadratic programming optimization algorithm. The morphing concept included changes in the wing planform and wing section shape with an extending spar and telescopic ribs mechanism. To allow high strains, natural rubber was the choice for the skin material, though the reductions in wing drag were not achieved due to the skin's flexibility. However, it was concluded that some improvements on the concept may lead to good results.

Some projects concerning telescopic wings using telescopic spars were also developed in the automotive field. In 1997, Czajkowski et al. [13] determined the viability of a composite telescopic wing for a roadable aircraft. A model was constructed consisting of three segments and represented one quarter of the wing. The composition of the main system included: two aluminum tubular telescopic spars, three skin/rib sections, a drive mechanism using a 12V motor for actuation, and a center box made of fiberglass and balsa wood sandwich plates. Based on results from a finite element model analysis made in NASTRAN and a functionality model it was concluded that telescopic principles can be successfully used from deployable highly loaded airfoil structures.

### 1.1.3. Recent design and development of telescopic wings

Mestrinho *et al* [12] developed and preliminary tested a variable span wing (VSW) actuated by a servo mechanism. Part of the study was focused in obtaining the optimal span values that minimize the drag to different operation speeds, achieving a reduction of 20% in the total drag in velocities close to 30m/s. Alongside this study, the rolling authority of the wing based on its asymmetrical deployment

compared to a conventional wing with ailerons was also determined. From this, a VSW wing prototype was designed and built for concept evaluation.

An aerodynamic shape configuration code developed by Gamboa [14] was used to determine a set of optimal wing shapes for reduced drag at a range of flight speeds. The results of this optimization demonstrated (in Fig. 1.5) that the VSW shows better performance (less drag) above 22.5 m/s than a rectangular wing designed with the same stall speed constraint. At 30 m/s, 40 m/s and 50 m/s a total wing drag reduction of 20%, 33% and 40%, respectively, was predicted. At low speeds, the VSW exhibits slightly more drag due to lower efficiency of the modified SG 6042 airfoil adopted.
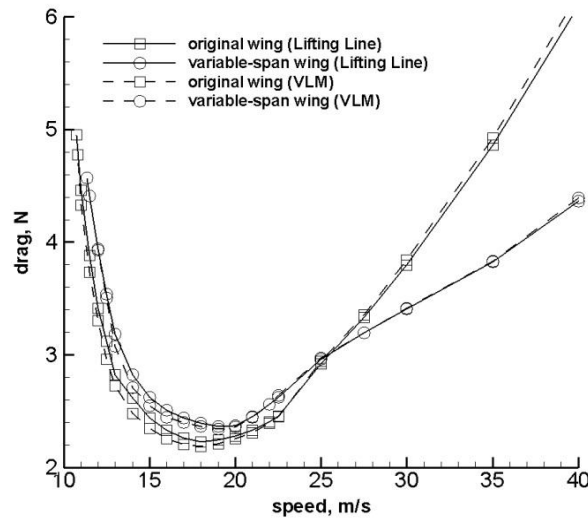


Figure 1.5 –Drag comparison between original and VSW.

The variations in wing span is not compatible with the use of conventional ailerons, thus, rolling maneuvers must to be controlled by asymmetrical span deployment. It was concluded that the wing showed enough rolling authority, as can be observed in the Fig. 1.6. This system differs from the conventional aileron once it decreases the rolling rate as the velocity increases.
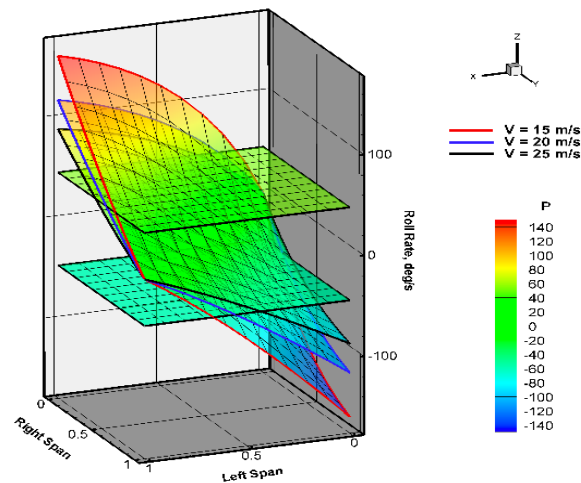


Figure 1.6 – Roll rate variation for flight speeds of 15, 20 and 25 m/s.

The prototype was sized based on the original wing used on the testbed UAV. Therefore, the maximum span was established at 2.5m and, from that, the fixed and movable wing parts were built with 0.625m permitting an overlap of 0.1m in its maximum extended position.

The outer movable wing (OMW) construction was based on a conventional method: balsawood ribs joined by a carbon tubular spar and covered by a carbon skin. As far as the fixed wing is concerned, it had to be hollow so that it could accommodate the movable wing. Consequently, it was made of carbon/epoxy and PVC foam sandwich reinforced with two carbon spar caps. The actuation mechanism was achieved through a modified servo system allowing a maximum deployment of 0.525m, although, it did not demonstrate enough torque to pull the movable wing. The final assembly mass was 1.54kg. Static loading tests carried out revealed an excessive torsion of the wing when loaded with a 9.8N load simulating 3.5g.



Figure 1.7 – VSW mounted on Olharapo's fuselage [ref].

Vale et al [11] designed a telescopic wing that enabled a 15N extra payload and a drag reduction between 1.7 and 12 N in a 100N takeoff weight aircraft. A computational analysis was performed that, apart from altering continuously its wingspan deploying an inner wing through a 750mm distance, also demonstrates airfoil shape change capability, going from a low speed airfoil (Eppler 434) to a high speed airfoil (NACA 0012). Figure 1.8 shows the wing's structure.

Carbon plates were used to guide the motion of the inner part of the wing which required that this moving part is an open section. The deployment sequence can be observed in Fig. 1.8.
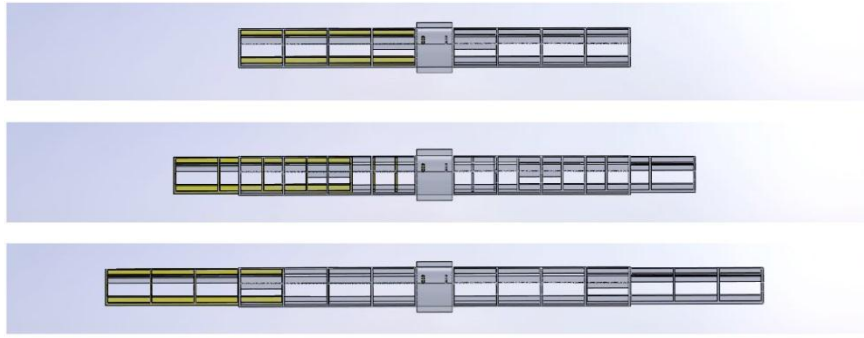
Figure 1.8 – Deployment sequence [11, page 4].

A prototype of the wing was built without the airfoil change due to construction limitations at the time. Thus, the NACA 0012 airfoil was adopted with inner and outer wing part chords of 210mm and 280 mm, respectively. The mechanism is actuated by electric motors attached to the inner wing and forcing it to slide along the wing spar and the guide plates in the leading and trailing edges. This method has the disadvantage of presenting open leading and trailing edges.

Ground tests were done to determine the wing's deployment times and the energy consumed by the actuation system. The results are shown in Table 1.2.

| Loading | Outer wing tip load (N) | Inner wing tip load (N) | Total deployment time (s) | Total retraction time (s) | Total deployment energy (J) | Total retraction energy (J) | Max current intensity (A) |
|---------|------------------------|------------------------|---------------------------|---------------------------|-----------------------------|-----------------------------|---------------------------|
| 0g | 0.0 | 0.0 | 17.0 | 17.5 | 58.14 | 59.85 | 0.57 |
| 1g | 16.0 | 9.0 | 18.0 | 18.5 | 71.28 | 73.26 | 0.66 |
| 1.5g | 24.0 | 13.5 | 19.5 | 20.0 | 84.83 | 87.00 | 0.88 |
| 2g | 32.0 | 18.0 | 21.5 | 22.5 | 110.30 | 115.43 | 1.14 |

Table 1.2 – Deployment test results [11, page 15].

Taking the results in consideration, it is possible to come to the conclusion that the roll control will not be possible because deployment times are quite large. As far as the energy consumption is concerned, it indicates that a 2200 mAh battery pack could maintain continuous actuation for at least 1.7h.

## 1.1.4. Inflatable wings

In 2003, Cadogan et al [15] focused his studies in significant advancements concerning deployable inflatable and rigidizable wing structures for UAV and other airship applications. Further developments [16] were based on wing warping to allow roll on inflatable wings. In order to modify the camber section (whose features included high response frequency, low power consumption, high

life cycle, among others) the following actuation methods were taken into consideration: piezoelectric actuators, electro-active polymers, shape memory alloys, pneumatic chambers, nastic cells and distributed motor-actuator assemblies.

A system capable of compact packaging for easy transportation and large damage tolerance became the main goal of a later study [7]. The aspect ratio morphing in two different situations was taken into account: one for packed systems which can be dropped or gun launched and deployed wings in flight, and other for a different kind of vehicles requiring aspect ratio changes to improve endurance. Inflatable wing structures show as its major advantage the possibility of close approximation to any wing shape, even those with camber. For low Reynolds numbers (Re < 500,000) a bumpy surface increased aerodynamic performance.

As Shape Memory Alloys (SMA) were promptly accessible and had the required stress and strain response, they corresponded to the most accurate choice for actuation purposes. Flight tests were performed with SMA wires to which a servo mechanism was added. Fast response times with significant wing deflection were accomplished, closer to a wing flap arrangement at the trailing edge.

The aeroelastic behavior of the inflatable wing, mainly twisting and bending, was evaluated through wing tunnel testing. The results were within the acceptable values. Through the comparison of a warping wing with traditional ailerons, roll moment coefficient and aileron control power were determined. The gradual deflection was partially responsible for the small over performance of the inflatable wing. Nevertheless, this increase is not observed when concerning the aileron control power.

Control tests were executed in order to determine the survivability of a coated fabric wing. These included: rapid deployment, 23 kg sand bag in two different areas of the wing, rapid inflation and flight impact. The absence of any kind of leakage alteration was crucial and confirmed by all tests performed. Thus, inflatable wings showed a high impact survivability, reusability and packability. They also actuated as a kind of airbag, absorbing the impact to other components of the aircraft, ensuring a robust behavior permitting an expanded flight envelope and less proficient piloting.

Inflatable wings were also presented by Jacob et al. A high altitude test [17] exhibited the feasibility of rugged inflatable wings for planetary exploration. The capability of power generation in multifunctional inflatable structures was proved when flexible solar cells were mounted on the wing surface. Aiming at determining the effects of aerodynamic loading and design options for warping actuation, a detailed finite element model of warping Vectran inflatable wings was presented.More recently, discussions have been taking place about the advantages and disadvantages of using this type of wings on UAVs. [18]

In t 2008, Kheong and Jacob [19] approached differently the aspect ratio morphing in flight using inflate wings. The study consisted in an inflatable wing made out of polyurethane fabric with a

rectangular form, a 36-inch semi-span from tip to root and a 13.5 inch chord. To each end of a rigid wing, using an NACA 4318 airfoil, an inflatable wing was attached, providing a 150% increase in aspect ratio. In terms of the study itself, two inflatable wings were considered, with and without the folding mechanism. Nevertheless, giving its reduced cost and simpler structural design, the study was focused on the second inflatable wing mentioned. In this case, instead of control surfaces, wing warping was used for roll control.

A flight test was performed taking into account two configurations: a dash one, using the inflatable wings rolled-up to the tips of the rigid wing; and a loiter configuration with the inflatable wing extended. A reduced deployment rate was obtained from the light-weight inflation system which can be positive to decrease the overall aircraft structural weight and strength of the rigid wing due to reduction of dynamic loads (high dynamic loads were experienced on the fuselage skin or rigid wing at high speed deployment) as it unfolds.

Both configurations were submitted to aerodynamic analysis and lift coefficients were predicted. The latter presented a 58% increase after the inflatable wings were deployed. The thrust required calculation displayed a fluctuation of 25% between low and high aspect ratios. A high aspect ratio wing, on the stall speed was beneficial since a reduction from 8.1 m/s to 4.8 m/s was accomplished. Also, some advantages were relevant in the rate of climb, as it was 16% higher when tested at 15.24m/s when compared with the low aspect ratio configuration. Wind tunnel testing revealed the influence of dynamic pressure on the inflatable wing during the inflation process.

## 1.1.5. Next Generation Morphing Aircraft Structures

Bowman et al [20] presented an overview of the work performed under the program DARPA/AFRL/NextGen Morphing Aircraft Structures (N-MAS). Three important aspects were approached in this overview: motives to morph, technology and systems development to increase the level of technological readiness and future work addressed to the technology progress, challenges concerning technology transition and systems integration.

Regarding the reasons for morphing, some theoretical approaches based on text-book formulas were enough to demonstrate that one must continue to invest in developing morphing technologies. However, in this project, studies and comparisons were made in a wind tunnel with realistic loads to obtain more reliable results. This analysis was based on fuel consumption and not on variables such as turn rate, takeoff distance, etc. After estimating the cost of operating an aircraft equipped with this technology, and cross-referencing the data with the number of sorties, it was concluded that for "hunter-killer" missions morphing technology does makes sense, even with 10% weight untapped,

especially for aircraft below 9080N. Another advantage of this technology is to reduce the aircraft fleet.

The requirement to make major changes in geometry of the wing led to the consideration of more than 20 different models, including telescopic wings, joined wings and fan wings. Of all the concepts generated the term "batwing" was chosen based on the following criteria: overall performance, estimated actuation power requirement, perceived ease of construction, feasibility of design, fabrication and testing within the project budget. The design adopted offers large geometry changes, including alterations in aspect ratio of 200%, 40% in span and 70% in wing area. Figure 1.9 illustrates the NextGen concept in different wing settings for five specific flight conditions.



| b/2 = 8.8 ft | b/2 = 9.8 ft | b/2 = 7.2 ft | b/2 = 9.8 ft | $b_{dash}/2$ = 7.2 ft |
| S = 17.0 sq-ft | S = 22.8 sq-ft | S = 15.8 sq-ft | S = 17.4 sq-ft | $S_{dash}$ = 23.9 sq-ft |
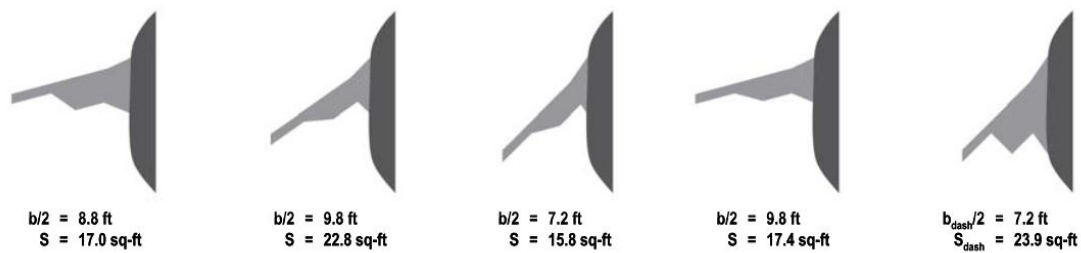
Figure 1.9 - Wing configurations for high-lift, climb, cruise, loiter, and maneuver [20, page 8].

This concept requires some revolutionary wing design tools and analyses as well as unconventional techniques and materials. An example is the skin of the wing that would be flexible enough to allow the change of geometry and which must be of sufficient strength to withstand the aerodynamic loads. Andersen et al [21] developed and tested in the wind tunnel the concept of in-plane moving geometry as well as flexible elastomeric skins. This study analyzed the kinematic-structure with a finite element model and also an aerodynamic consistent model with MSC/NASTRAN™ to assess its aeroelastic behavior.

A model of the batwing concept with the following characteristics: a total weight of 500 kg; wing variable sweep from 15 to 45 degrees, variable wing area from 1.4 $m^2$ to 2.4 $m^2$, and the half-variable span from 2.1 to 3 m, was tested in wind tunnel. These tests had three major objectives: establishing the overall structural integrity of the design by testing it at loads up 2.5g, demonstrating the capability to morph at 1g conditions, and correlating with predictions.

In addition, Flagan et al [22], as a proof-of-concept demonstration, developed and successfully flight tested a 45 kg jet-powered RC (named MFX-1) with the batwing concept. The model flew at altitudes between 122 and 183 m at speeds from 51 to 62 m/s. On this model, the wing area was altered 40 %, the wing span 30 % and the wing sweep varied from 15 to 35 degrees. During the flight, less than 15 seconds were needed in order to achieve a successful morphing cycle.

### 1.1.6. Fully Adaptive Model

The design and construction of a fully adaptive aircraft configuration was managed by Neal et al [23] as an experimenting testbed for aerodynamic modeling and flight control. The aim of the adaptive model design was to achieve several changes concerning shape, so that, morphing for multi-mission UAVs could be explored. These changes were expanded to five independent planform shapes along with the independent twist control for each wing.

The actuation system was composed by two rotational actuators for wing twist and five linear actuators to control wing shape (pneumatic actuators for tail and wing extensions, and a lead-screw mechanism for sweep actuation were used. The control and data acquisition circuit used PC/104 boards and a Matlab/Simulink environment.

The aerodynamic features were evaluated when the 7-DOF experimental model was tested in wind tunnel, with particular attention on the aerodynamic center location and the drag force. It was concluded that, for a span extension of 0%, 50% and 100% the aerodynamic center shifted 19.5%, 22.3% and 25.7%, respectively. The influence of the planform variation was estimated on aircraft stability. It was determined that the CG variation was 11% from an unswept condition to a fully swept one. This indicated that, by increasing the sweep, the aircraft became more stable.

## 1.2 Objectives

The objectives of this work consisted in the construction and testing an experimental telescopic span wing, actuated by a simple rack and pinion electro-mechanical system, for further application on the UAV Olharapo. Also, the improvement of the 2009's prototype was taken into account.
The next topics had to be accomplished in order to achieve the goals described:

    I.    Figure out a solution which improved the sliding between the IFW and OMW.
   II.    Development a system so that the VSW actuates quickly and reliably
  III.    Study the most applicable construction methods.
  IV.    Perform bench tests in order to assess the functioning mechanism

## 1.3 Dissertation layout

The thesis begins with an introduction on morphing concepts and with particular focus on large scale span change studies and experiments. A review on UAV's equipped with morphing technology is also performed.

The dissertation is divided into four main parts: existing VSW prototype evaluation (Chapter 2); design and construction of a new prototype (Chapter 3); VSW evaluation and results (Chapter 4); and a summary (Chapter 5).

Chapter 2 presents the 2009's prototype issues, as well as the hypotheses and corrective measures.

Chapter 3 describes the detailed exposition of the new VSW's overall construction, including some construction methods evaluation and experiments.

Chapter 4 reports the various tests performed, results and evaluation.

Chapter 5 presents the overall conclusions as well as future work and recommendations.

# Chapter 2

# Existing VSW Prototype Evaluation

The VSW prototype implemented by Mestrinho et al [Ref] exhibited some flaws at different levels. Therefore, the first approach to this work was to improve the initial prototype, evaluate its operation and then build the second wing by applying the knowledge gained in the process.

## 2.1. Issues of 2009's prototype

At the beginning of this work, the existing prototype presented several problems that required attention:

   i.   When loaded, the wing showed an excessive torsion (see Fig. 2.1);

   ii.  The actuation mechanism was not strong enough to make the OMW displacement (Fig. 2.2);

   iii. The actuation rack was undersized for the actuation force necessary;

   iv.  The construction method induced some defects in the IFW's carbon layers (see Fig. 2.3).



a)                                                    b)
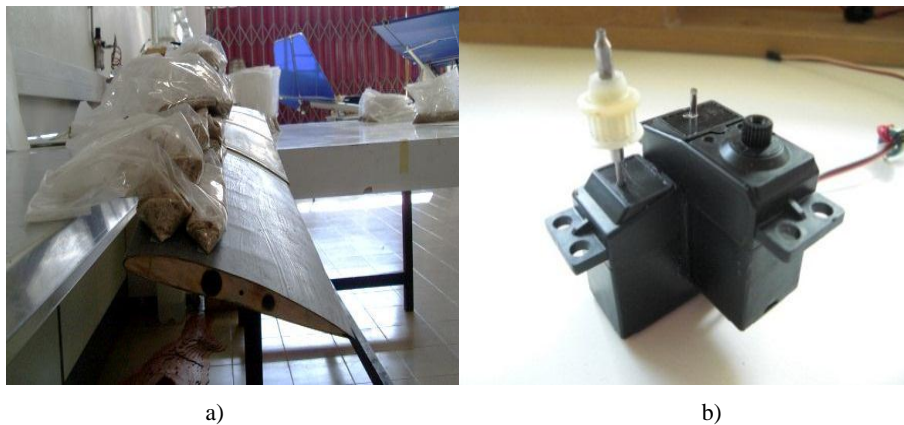
Figure 2.1 and 2.2 – VSW on bench test and servo mechanism respectively.

Figure 2.3 – Bubbles and wrinkles on IFW's surface

## 2.2. Hypotheses and corrective measures

### 2.2.1. Excessive torsion of the wing

The excessive torsion of the wing was due to the lack of stiffness at the trailing edge where the upper and lower skins are joined together. This problem was solved by attaching a triangular profile of balsawood with two layers of carbon/epoxy composite, one on the top side and another on the bottom side, to reinforce the trailing edge thus making the structure into a fully closed section.

### 2.2.2. Actuation mechanism strength and speed

The actuation servo used in this prototype was a modified ordinary servo that, instead of spinning 2/3 of a turn, or more exactly 210º, would spin sufficient turns to push the OMW through its full extension in time for an effective rolling control. Thus, a compromise between speed and torque was necessary. The servo used was a Futaba S3001 with extra reduction stages added to alter the feedback relation in the potentiometer and the actuation axle repositioned to adjust the number ot turns. These changes have negatively affected the torque that the system could produce. In this specific situation, the torque obtained failed to overcome the friction between the IFW and OMW surfaces.

The solution to this problem would be to use more powerful servos and find another way to achieve the necessary displacement.

### 2.2.3. Rack instability

The new torque values were useful to understand that the rack in use presented excessive torsion when pushed, working in compression, leading to teeth sliding on the pinion.

Having said that, the rack material would have to be changed in a way that it resists buckling and torsion created during the OMW's outward motion.

### 2.2.4. Construction defects

The method used to laminate the carbon skins around the PVC foam caused some imperfections which affected the proper sliding to the OMW. In addition, from a structural and aerodynamic point of view, these surface defects are not desirable.

A new construction approach would have to be considered so that all types of friction between the VSW's moving parts were reduced and structural discontinuities were minimized.

## 2.3. Improvements made in 2009's prototype

The main problems of the 2009's prototype were the excessive friction between the wing surfaces and exaggerated twist observed in the bending test. Therefore, the main concern was to reduce the sources of friction as much as possible and effectively close the trailing edge. This friction had as main causes the resistance generated between the outer surface of the OMW and the inner surface of the IFW and some imperfections of construction, including ribs with slight differences that altered the thickness of the profile in specific areas of the OMW. To correct the rib's problem, the carbon skin in these areas was cut and removed. The ribs were trimmed, a small rectangle to cover the cut was laminated. Still, these patches did not comply with the desired perfection.

Some ideas were considered to place ball bearings in the system in order to improve the sliding. From the beginning there were several requirements for this system: it had to have an adjustable slack and easy access to facilitate assembly/disassembly of the wing.

A ball bearing rolling device, included in the OMW tubular spar, which slides in an L or T section track would be glued to the inner surface of the IFW, which would illustrate an elegant option. However this system raised several issues on this scale, the bearings could not have more than 3-4 mm in diameter and had to placed within the structure of OMW in an area of difficult access for relaying slacks. Another relevant problem was the fact that OMW needs an opening in the tubular spar to accommodate the track where the ball bearings slide thus converting the tubular spar to a C section beam.

A second option would be to use a system of linear bearings, this system would be mounted on the OMW tubular spar allowing the tube IFW slide within the bearing, permitting a relatively simple implementation. This method was not chosen since most of the IFW's efforts are supported by the shell and not the tube, which serves mostly as a guide. Therefore, the option to include any bearings would require them to pass through the shell of the IFW.

The third option reached the best compromise between simplicity, access, reduction of friction and load transmission. The main objective was to put the OMW sliding inside the IFW without the two surfaces come into contact, or reduce the contact area to a minimum. The system consists of a set of six bearings divided into two groups. A pair of bearings on the trailing edge, keeping a small slack to allow the trailing edge of OMW to slide without touching nothing more than the two bearings. The other two pairs were placed in the IFW's shell over the center of pressure of OMW, though its position was slightly offset so as not to puncture the stringer of the IFW.

This system was implemented and tested in the original VSW prototype. For this analysis we made some changes, particularly in the structure of OMW and the shell of the IFW. Since loads are transmitted only through the areas of contact between the OMW and the bearing those areas had to be strengthened. In order for a smooth sliding motion to be obtained, the bearings cannot slide directly onto the carbon skin of OMW. Thus, it was necessary to reinforce the OMW carbon skin in the areas of contact with the ball bearings. This strengthening consisted of placing two rectangular tensors made of pultruded carbon on which the bearings slide to ensure sufficient rigidity of the skin of OMW in that particular area.

## 2.4. Tests

After mounting the bearing system, improvements were evident in the reduction of friction (about 40% improvement) even though, the actuation system developed was not able to perform the deployment on a test bench. The reasons for that were two: the low torque provided by the servo

actuator, mainly due to the reduction of gear stages used, and the imperfections on the surfaces in contact.

A second test was carried out where an original servo (without reduction gear) was mounted in the system to evaluate the interaction of all components. The result of this test was not as good as expected. The rack used had not sufficient strength to withstand the forces involved, a new solution remain to be found. Another test was also made to determine the force required for a complete deployment of the OMW. After this test, it was established that a 16. 7N force was needed for a complete deployment without any wing loading.

## 2.5. Conclusions

After the improvements and tests were performed some conclusions essential to the success of a new prototype were drawn. Starting with the actuation system, a more powerful servo was required to perform a successful deployment and a new  system of rack and pinion had do be sized and built. The method of construction and the stiffness of the OMW in the area of contact with the bearings had also have to be improved.

# Chapter3

## Design and Construction of a New VSW Prototype

The concept of the VSW in this project is presented as a hollow fixed wing in which a movable inner wing slides. Dimensions such as wingspan and chord, airfoil, and major structures were maintained from the 2009's prototype, since the first approach was to improve the original VSW and build the respective pair.

The evaluation of the first VSW's functionality led to the conclusion that it was crucial to significantly improve the sliding motion between the IFW and OMW. The purpose was to reduce friction so that the actuation mechanism was able to make an effective deployment, even under wing loadings up to 4g. The primary ideas included the insertion of bearings in order to facilitate sliding and improve the method for lamination of fiber layers so that a uniform bonding was guaranteed.

The entire structural design accomplished in the previous work was adopted. In this work, the efforts were centered on validating methods of construction, creating a new actuation system, finishing the construction and testing a pair of the completed and functional wings.

## 3.1 Preliminary considerations of the manufacturing process

For a suitable lamination and good surface quality, had-layup and vacuum bagging lamination was chosen, since this technique allows a lightweight structure, low cost and reduced complexity. In fact, this procedure allowed drawing much of the resin in excess, prevented air bubbles in the carbon layer and a satisfactory finishing. Briefly, this method consisted in putting the carbon/epoxy in the mold previously protected with wax as releasing agent. Then, a layer of peel-ply was placed, whose function was to provide an ideal finishing for future bonding. Then, the release film was applied and finally a layer of breather. This set was then involved with a film, which after sealed with a vacuum joint, made it air tight. Then, it was just necessary to connect a vacuum pump to the sealed film in order to remove air from the interior.
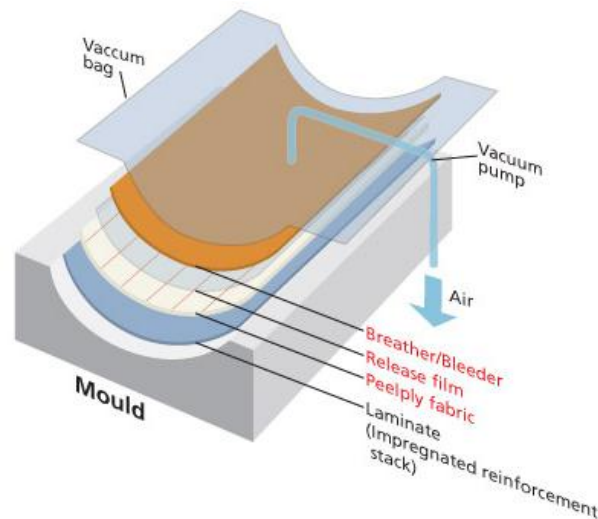
Figure 3.1 – Scheme of the various materials involved in the vacuum lamination.[http://www.fibertex.com/en-GB/business-areas/Composites/Compoflex/Products/Pages/Products.aspx]

The cure process was performed under controlled temperature conditions, consisting in cure and post-cure. The resin used was SR 1500, which can be used with various hardeners. However, the hardener available was SD 2503, considered a slow one. The manufacturer indicates that the hardener should be used for standard laminations and for all types of applications, having a working times of about 47 minutes at 25 °C. Thus, it appeared to be the suitable hardener for the desired application. Regarding the curing process, the procedure required by the manufacturer, 24 hours at 20 ° C, was performed. After this time, the composite entered in the process of post-cure. There are basically three procedures to perform the post-cure: 14 days at 20 °C, 24 hours at 40 °C or 16 hours at 60 °C. A post cure at 60 °C would be risky because it could damage the various molds used. So, the second procedure was chosen because it was one that combined the best compromise. This procedure was used for all composite fabrications that have been undertaken. In order for the mechanical properties of the composites were known and properly controlled, the performance of the curing process and proper post-curing was extremely important.

## 3.2 Outer Movable Wing (OMW)

The OMW's dimensions were maintained so that its wingspan measured 525 mm and a 100 mm overlap when fully extended was obtained, achieving a total of 625 mm for its length.

The need for a smoother, but at the same time more rigid structure in the zone of contact with the bearings, led to some structural changes on the initial OMW. Two stringers of pultruded carbon fiber

in the mentioned zone of contact were placed, and later, a 1.5mm balsa web was attached to prevent surface's deformation, resulting from the force transmitted by the bearings. The set including the stringers and the balsa formed an I-beam, where the stringers were the flanges and the balsa represented the web (see Fig. 3.2). This alteration would substantially increase the bending strength with minimal gain in weight (about 15 grams).



<div align="center">(a)                  (b)</div>
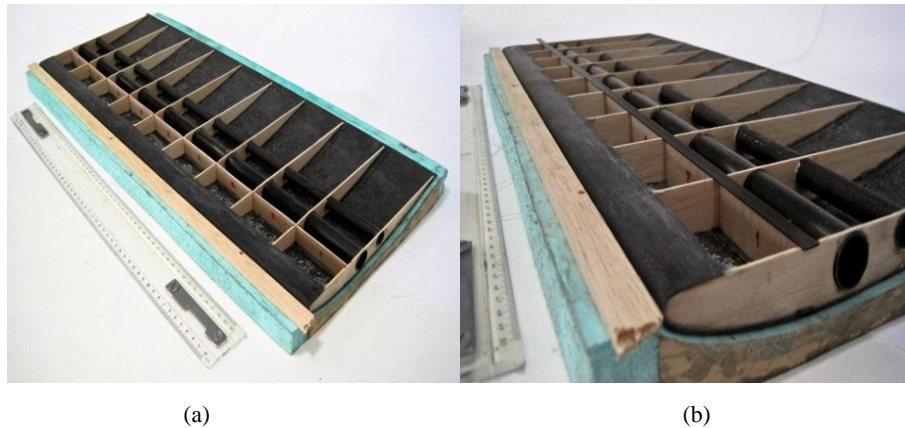
Figure 3.2 – Construction detail of (a) the balsa web and (b) the carbon flange..

Several construction methods were taken into account, such as autoclave, vacuum bagging and the previous method referred in [14]. Aiming to maintain the reduced weight as well as good fitting between the OMW and the IFW, it was decided to use the vacuum bagging lamination.



Figure 3.3 – Vacuum bagging final installation.

The lamination vacuum was employed in the manufacture of the OMW's shell, and, for this, an external mold was used (Fig. 3.3), made from an internal mold, which would also serve to create the

IFW thus providing a fitting in the tolerances between OMW and IFW. In order to avoid extra weight, the stage of lamination of OMW's skin included already with the upper skin stringer in position.



Figure 3.4 – External mold used to manufacture OMW's shell.

The ribs were built in 2mm thick balsa wood. Since the OMW's skin shape depended on the ribs, this step was crucial to obtain a regular surface, providing low resistance in the IFW's entrance. Thus, a mold was made to allow the manufacture of all ribs at once and with imperceptible differences between them. As noted in the Fig. 3.5, the mould had two lumps in the area where the tubular spar would cross. This feature preserved the ribs integrity and shape during the construction process.



Figure 3.5 – Ribs cutting mold.

Later, the ribs were drilled to accommodate the spar and the rack's guide tube. The spar consisted of a pultruded carbon tube. Pultruded carbon tubes combine the best compromise between availability,

price and specific strength. As for the guide tube, since it is not a structural element, it only had to maintain its integrity and guide the rack of the opposite OMW through the ribs. This tube was built in bidirectional carbon using a PVC pipe as a mold with an outer diameter of 12mm. In the construction process two techniques were tested: (a) the vacuum bagging and (b) by wrapping the carbon around the tube by pressing it with tape to secure the tubular shape. Of the two methods, the second was the one that produced better results since method (a) caused wrinkling in the layers of carbon. The results are shown in Fig. 3.6



Figure 3.6 – Demonstration of the results using technique (a) (right) and (b) (left).

The step of attaching the ribs to the skin was critical, since the slightest imperfection would deform the wing and hinder the entry of the same within the IFW. Therefore, a dock was built (see Fig. 3.7) to ensure the intended shape after collage. As a method of construction, it was chosen a manufacture in expanded polystyrene cut with hot wire. This option was based on the speed of construction combined with the quality of the final result.



(a)                                                                                          (b)
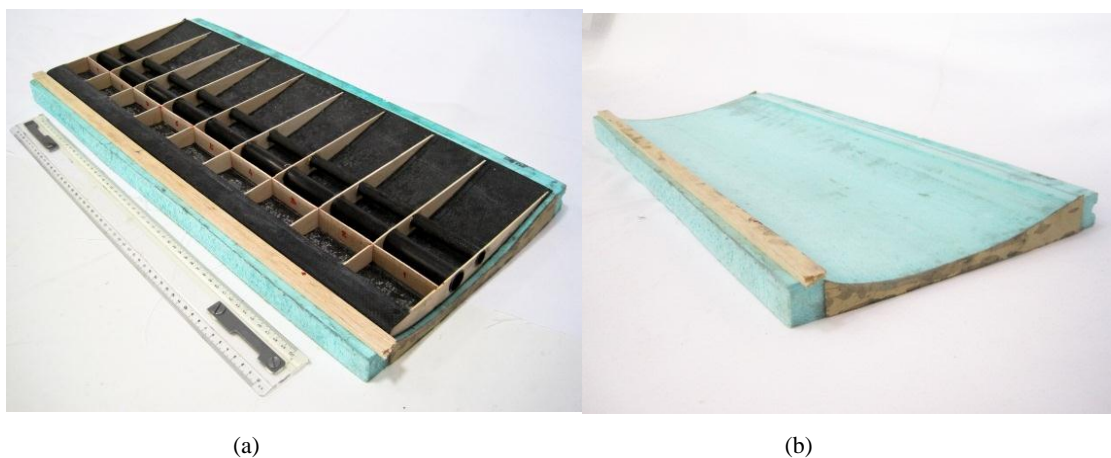
Figure 3.7 – Construction (a) step and (b) dock.

At this stage, the balsa plates were added and, in order to increase stiffness, they were placed with the fibers perpendicular to the spar. Later, the lower skin stringer was placed. This set was closed with a flat layer of carbon.
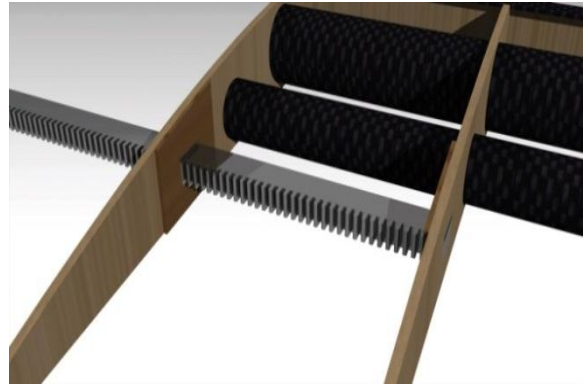


Figure 3.8 – Detail view of the rack supported by OMW's structure (CAD drawing).

After assembling the final set there was a slight misalignment between racks and guide tubes, which blocked the complete retraction of OMW. In order to reverse the situation, an alignment cone was added in the guide tubes, allowing the rack to follow the desired path. This led to a good retraction.

## 3.3 Inner fixed wing (IFW)

In this wing, the necessity of obtaining a hollow structure required a structural approach different from the movable wing. So, the whole skin and webless spars of the IFW would not only maintain its shape and resist bending but would also receive the resulting forces transmitted from the OMW when extended.

Taking these restrictions into account, an unusual setting was adopted since the IFW's skin was composed by a sandwich of two layers of carbon with 195 g/m2 and expanded PVC foam in between with a density of 55 kg/m$^3$.

As for the spar, it was composed by two rectangular beams made of pultruded carbon with a cross section of 1.8mm x1.8 mm. For greater rigidity of the set, it was decided to build the spar with the size needed, avoiding unnecessary stress concentrations. These beams had a length of 1600 mm. However, as the dimensions needed were not available, existing only in $1000 \times 9 \times 0.9$ mm, a carbon beam was constructed based on these. Note that these tensors were made of pultruded carbon thus eight of these beams were attached, taking into account the mismatches of all joints in order to minimize the risk of failure. Chamfers were also used in all joints, following the proportion of 1/12.

As a support to the bearings, aluminum plates were embedded in the structure thereby effectively distributing the loads transmitted by the set of bearings.

The method of construction adopted was, once again, the vacuum bagging, and in order to build a single skin three phases were necessary. The other option would be to laminate the entire set (carbon/foam/carbon) at once. However, this option was not feasible, given the complexity of interaction between the various impregnated materials. Doing all the steps in one would not make it possible to control the process and ensure the perfection desired. Thus the three phases were (a) to laminate the first carbon layer around the mould, (b) to mark the carbon layer, fold and attach the PVC foam, spars and the aluminum plates to support the bearings in suitable areas, and finally (c) to adjust the discontinuities and laminate the last carbon layer.

a) *Phase* 1

In the first phase, it was desirable to obtain a surface as smooth as possible so that the OMW's sliding was improved. Thus, all wrinkles and bubbles between the mold and carbon layer, as well as irregularities on the mold surface were inconvenient.

Since it was necessary to have a small slack between the outer surface of the OMW and the interior of the IFW, at a first approach a 0.1 mm thick plastic film was placed for this purpose. During the process, the loose plastic was not considered very practical, so, for future purposes, an adhesive film should be used in order to confer thickness to the mould, function as release agent. The final result, once only one layer of bidirectional carbon was used, presented gaps in the empty spaces between the fabric fibers. To overcome this problem it would have to be used a very thin layer of fiber (carbon or glass) to cover these gaps. This step was crucial to a successful phase two, because if the glue seeps through the holes in the skin, it would not join the PVC foam effectively.
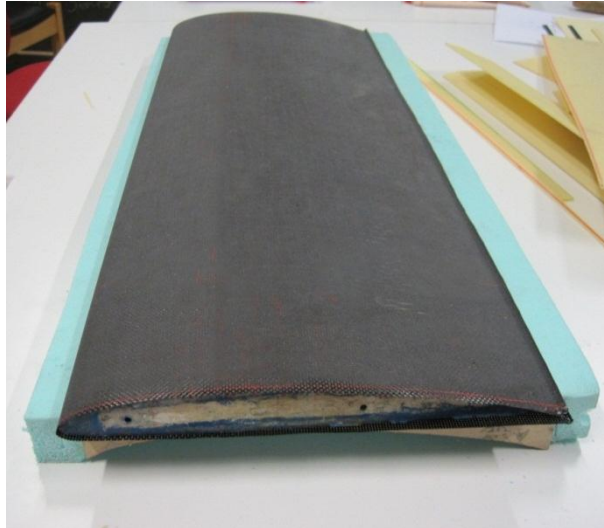
Figure 3.9 – First carbon layer after phase 1.

b) *Phase* 2

To attach the PVC foam to the carbon layer, tests were performed using epoxy glues of different viscosities (SR 1500 SR 7300 Aerobound with a viscosity of 700 mPa.s and 40000-45000 mPa.s respectively) to obtain the best adhesion from the carbon to the foam. It was concluded after these tests that it would be better to spread the most viscous epoxy glue (aerobound SR 7300) in both the carbon surface and a small, but uniform, layer of glue on the PVC foam. Simultaneously, it presented less maximum resistance, 70 N/mm2 (SR 1500/SD 2503) against 25 N/mm2 (Aerobound SR 7300).

The final properties vary according to the cure process. Taking into account the glue's features, the SR 1500/SD 2503 was expected to exhibit a more consistent bond though that was not the final result (Fig. 3.10). The reason for this poor outcome was the lower viscosity of the mentioned epoxy glue, allowing the PVC foam to absorb it and its leakage through the first carbon layer.

Figure 3.10 – Outcome after the use of epoxy resin SR1500 / SD2503 in the interface carbon-PVC foam.

Once an effective method for bonding was defined, the skin markings were made taking into account the size and positioning of the spars, aluminum plates to support the bearing and PVC foam (see Fig. 3.11).



(a)                                                                                          (b)

Figure 3.11 – Skin during the second phase (a) with marks and aluminum plates in position and (b) skin after conclusion of phase 2.

At this stage, a critical step, already mentioned in Chapter 2, was the of the PVC foam forming compliantly to leading edge. To that end, the foam had to be hot bent. At this point two methods were evaluated: (1) foam heated with hot air and (2) foam heated with hot water. Method (1) showed some imperfections in forming due to a large local heating. Method (2), thanks to the thermal stability of water, managed to maintain a uniform heat distribution across the length of the fold, resulting in a uniform and constant curvature. After folding, the foam was cut into three pieces as needed. The three pieces were attached together followed by the spars and the aluminum plates.
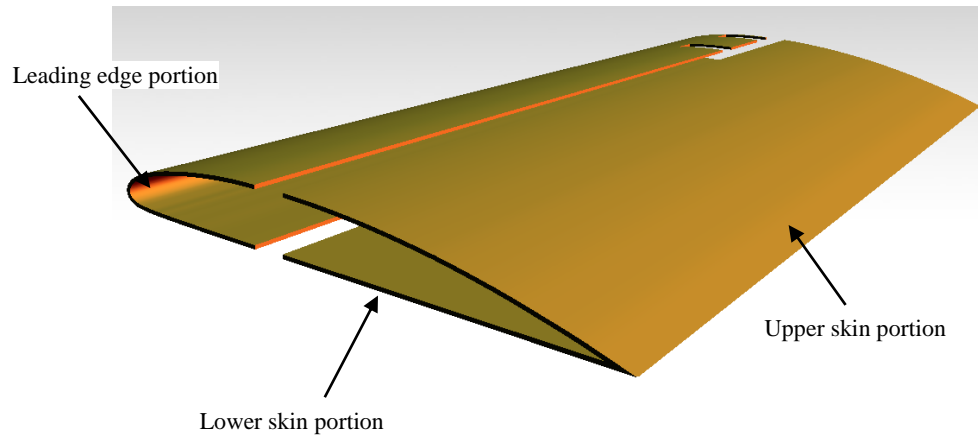
Figure 3.12 – Parts of the PVC foam.

c) *Phase* 3

After gluing the foam onto the first carbon fiber layer, it was necessary to eliminate the discontinuities between this and the spars since their thicknesses differed about 0.2 mm. Therefore, a filler material with a mass of 0.4 g/cm3 was used. To follow up these adjustments, one layer of carbon ($240 \ g/m^2$) a layer a fiber glass ($90 \ g/m^2$) were laminated on top of the spar to ensure the absence of gaps and a good finish.



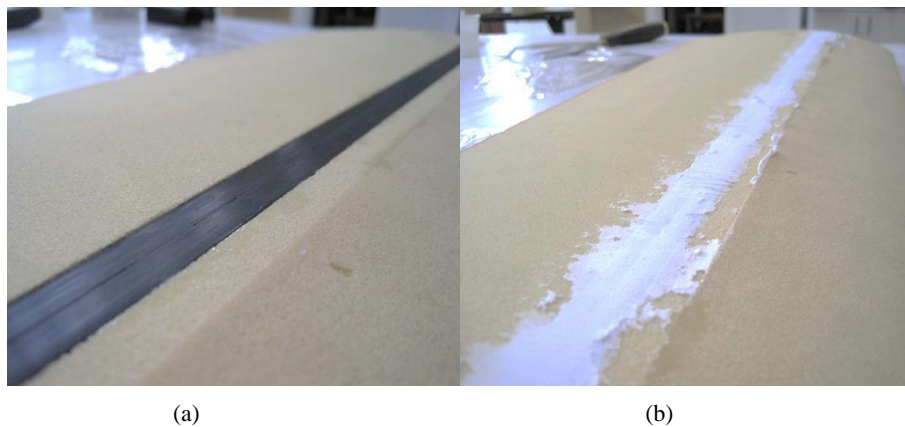(a)                                    (b)

Figure 3.13 – Picture of the skin (a) in the beginning of phase 3 and (b) after application of the filler material.

Figures 3.15 – Picture of the skin after phase 3.

All the results obtained, through the three phases described, showed improvements comparing with a previous experience in which it was possible to notice some problems relating the bonding between the PVC foam and the carbon fiber. This issue was due to excessive resin absorption by the PVC foam and drained glue through gaps in the carbon layer. Since the different layers were not attached properly, the outcome was not resistant enough. Some amends were tried so that the worst imperfections (figure X) would be repaired, though the result was not satisfactory.


Figure 3.16 – Corrections made on the previous IFW.

This was solved by using glue with a higher viscosity and putting a very thin fiber glass in the interior surface of the carbon layer, from what resulted the following sandwich sequence: glass – carbon – PVC foam – carbon – glass.


# 3.4 Actuation Mechanism

Given that this system was also required to control aircraft rolling, the actuation should occur continuously rather than focusing on a one-time deployment. Thus, during the previous work several actuation options were evaluated, leading to the choice of using a servo motor. This option took into account several factors such as availability, price, weight, simplicity of construction, feasibility and control. In future work, a possible development of an automatic span extension controller should be facilitated by this choice. Another advantage of using the servo motor is the ease of being controlled through a common radio transmitter used in aero modeling. The mechanism consisted of a set rack/pinion actuated by a servo motor.


## 3.4.1 Set rack/pinion

As stated in Chapter 2, due to torque values needed for proper wing deployment, the material and sizing of the rack had to be revised. Several factors were evaluated, weight, availability, size and price. After searching the market the following options were available: a rack in reinforced plastic (standard), in aluminum (per order) or in steel (standard). As far as the price was concerned, the plastic rack would be the best option, though it does not exist in the market with the desired dimensions. The aluminum rack would have to be ordered, though all budgets asked were quite high.
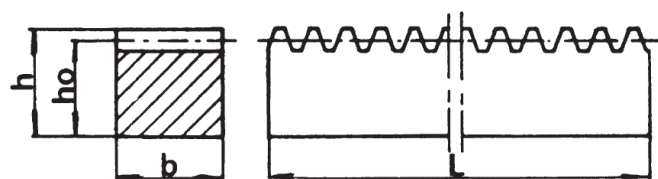


Figure 3.17 – Generic view of the rack [http://www.chiaravalli.it/home/index_en.htm]


It was decided to purchase a standard rack in steel with the dimensions 15mm x 15mm x 2000mm (b x h0 x L), and a module of 1mm, later to be cut into desired dimensions (5mm x 5mm x 800mm). Since the steel had superior strength relative to aluminum, a section of smaller dimensions could be used, thus approaching the weight of both options (and avoiding a large increase in weight). In Fig. 3.18 the

original steel rack with small sections cut from it can be observed. These cuts were made in a cold milling machine.



Figure 3.18 – From right to left: original rack, rack with the desired length and rack with the desired cross section.

As shown in Fig. 3.18, after cutting, the rack suffered significant bending. The stresses produced during cooling of the steel during manufacturing is the possible reason for that behavior. Thus, when cut, the steel tended to bend toward the original exterior face. Noting this fact, the only possibility left was to purchase a rack of aluminum per order. The rack used a section of 9mm x 5mm and a length of 800mm. The main problems observed in the experiment with the prototype in 2009 were (a) buckling of the rack and (b) the pinion sliding through the teeth of the rack. Problem (a) was solved by replacing the balsa rack for an aluminum rack. However, and since this was a critical system for roll control, some buckling calculations were made. Calculations based on reference [27] revealed that a section of 3mm x 3mm was sufficient for an ideal static application. Nevertheless, given that the rack as well as being a critical point of control, acted asymmetrically, it was included in a dynamic system and submitted to vibrations. Adding to the construction issues, a section of 9mm x5mm was chosen.

The pinion sliding on the rack (b) has occurred for two reasons. First, the material in which was made of (rubber) has low rigidity and therefore can easily deform allowing the pinion's teeth to slip. Second, the teeth were too small for the force evolved in actuation. These problems were overcome by changing the material (from rubber to aluminum) and increasing the tooth module to 1 mm.
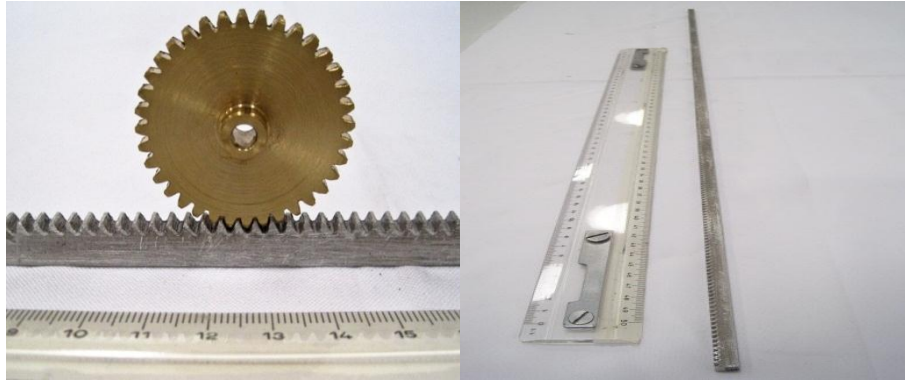
Figure 3.19 – Rack and pinion (left) and rack (right).

### 3.4.2 Servo motor

In the initial design Futaba S5301 servos were used since they were readily available and had the desired characteristics. In order to increase the servo travel, some modifications and tests were performed, leading to an useless servo. It was essential the equivalence between servos so another model had been considered. When choosing the new servos, several factors had to be considered such as availability, low price, high speed, high torque, low weight and metal gears, being the latter a prerequisite to carry out the necessary modifications. Combining the best compromise, a pair of Hitec HS-805MG servos was purchased.
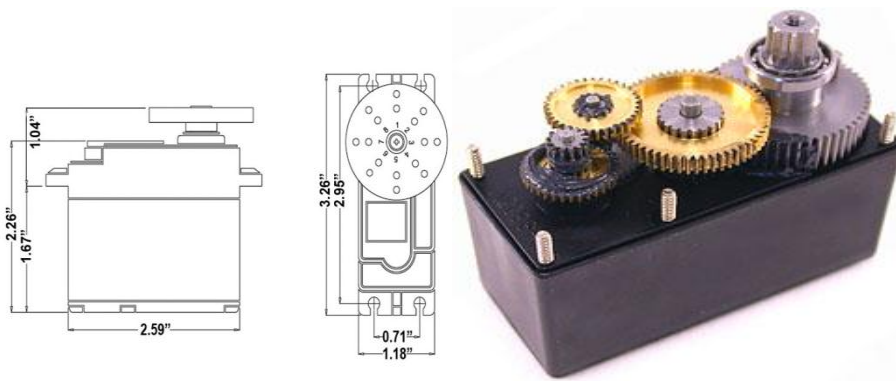


Figure 3.20 – Servo HS-805MG, views (left) and open servo (right).

| Motor Type: | 3 Pole Ferrite | |
|---|---|---|
| **Current** | 4,8V | 6,0V |
| **Speed (4.8V/6.0V):** | 316 deg/sec | 429 $deg/sec$ |
| **Torque, kg.cm (4.8V/6.0V)** | 19.8 | 24.7 |
| **Size, mm** | 65.79 x 29.97 x 57.4 | |
| **Weight, g** | 197.03 | |
| **Motor Type:** | 3 Pole Ferrite | |

Table 3.1 – Characteristics of HS-805MG servo.

The servo speed, being fast to common use ($429\ deg/sec$), was not enough for this application. The pinion perimeter was 113.1 mm and 4.6 turns were required (1672.6º), taking 4.2 seconds, to make a complete deployment with a $134,5\ N$ force.

Taking into account the relationship between the 1st and 2nd stages of the servo gears (Fig. 3.21) (gear ratio of 0.385) gave a speed and torque $1111\ deg/s$ and $0,93Nm$, respectively. This modification allowed an ideal complete deployment in 1.5 seconds with a $51,97\ N$ force on the rack which was better suited for the application. However, it was necessary to work out a solution to transmit the servo force to the pinion effectively and with little damage to the servo.
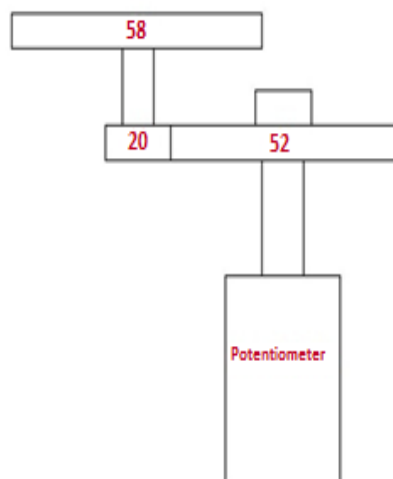


Figure 3.21 – Original potentiometer to servo configuration. The red numbers indicate the number of gear's teeth.

The solution to engage the pinion to the 2nd stage of transmission of the servo was a steel structure, lathe machined, that fit perfectly in the spur gear recess of the 2nd stage. The shaft, 4mm in diameter, is an integral part of the same piece, and is supported by two ball bearings, improving its alignment with the center. In Fig. 3.22 the cut piece as well as the final assembly can be seen.

(a)             (b)             (c)

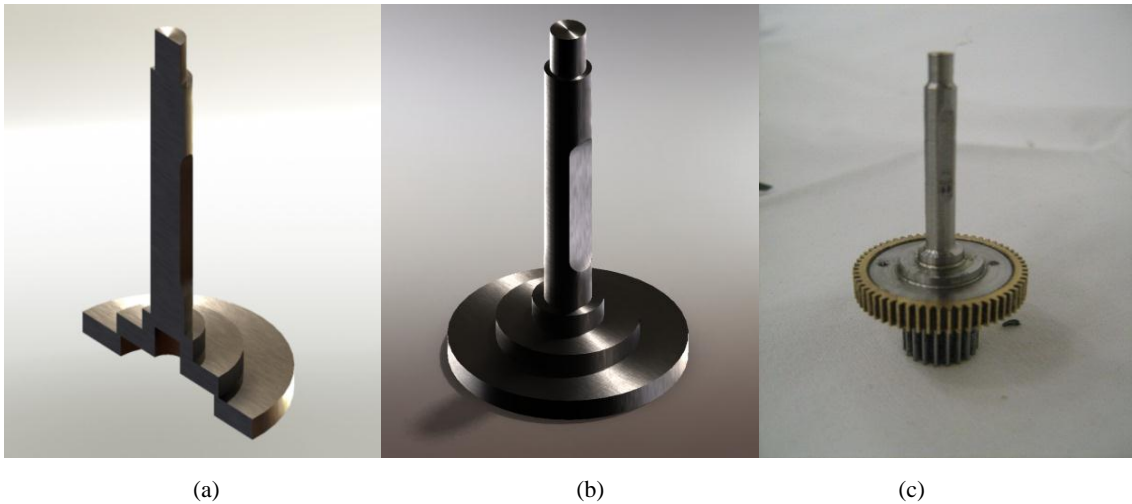Figure 3.22 – Servo's shaft cutting view (a), servo's shaft (d) and real servo shaft mounted on the gear (c)

To ensure the pinion was well attached to the shaft a plane side was opened on the shaft where a M2 screw makes pressure. Also to resist the torsion moment between the servo and the shaft, two 1.7 mm holes were made inside of which two steel pins were placed to ensure that the shaft would not slip under the actuation forces.

Having done that, attention was turned to increase the servo travel, since the original servo turned only 110º in the 1st stage. A relationship had to be found that converted the 1672.6º in 110º of the potentiometer feedback. This effect required a total reduction ratio of 0.0658 and so, four gears drawn from a set of gears in a S3003 servo were used, with a reduction ratio of 0.45 each. This assembly allowed an overall reduction ratio of 0.0617, which was enough for this application.
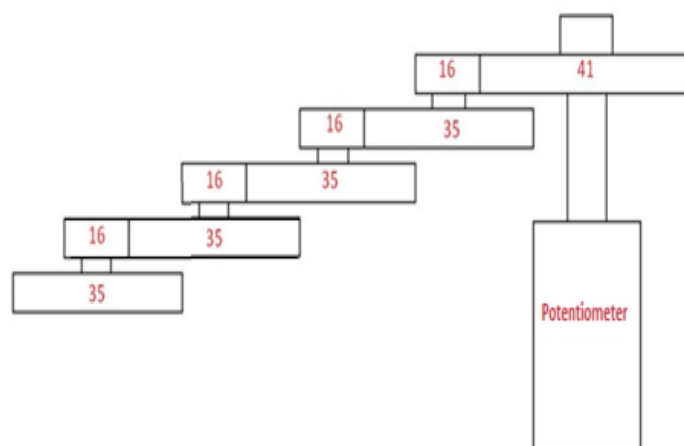


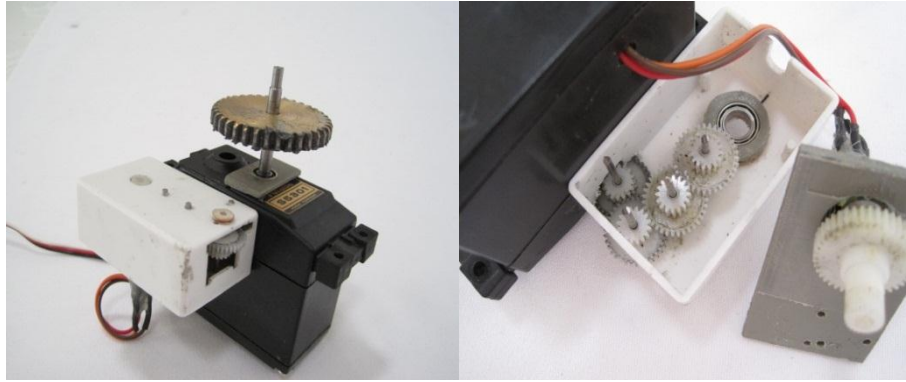Figure 3.23 – Diagram of reduction stages.

Figure 3.24 – Detailed views of reduction stages.

## 3.5 Wing's central structure

After the actuator system was developed, it was necessary to build a platform capable of supporting the servos and effectively transmitting the forces between them and the VSW, subject to geometric constraints dictated by the fuselage size of the UAV. Considering all this, the result was a plywood board 3 mm thick, supported by two brackets of the same material. These were glued to the wing tube and the spars, as seen in Fig. 3.25. Note that the alignment tube only extended up to the end of the plywood rib unlike the prototype initially proposed. This change was required due to excessive friction between the movable wing tube and the alignment tube.
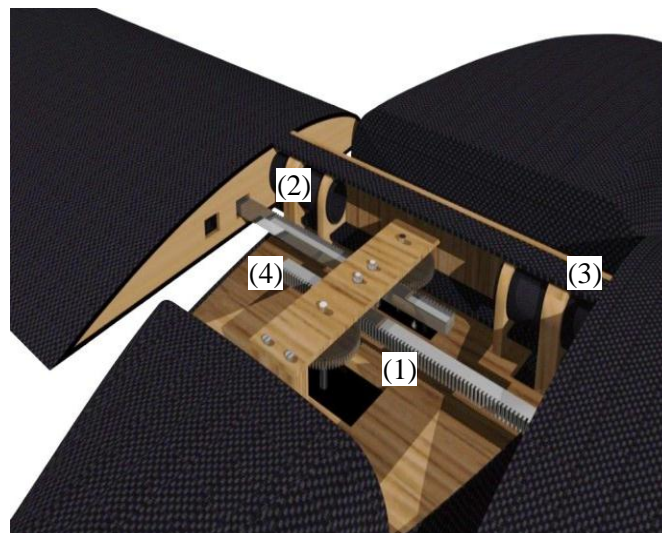


Figure 3.25 – Central fuselage part: 1) support board, 2) board linkage, 3) wing-fuselage connection and 4) upper board (CAD drawing).

In Fig. 3.25, the upper board (4) supports the pinions' shafts and the rack's rollers. The rollers function is to keep the rack in contact with the pinion teeth and restrict their vertical movement. In order to

reduce friction to an acceptable minimum, ball bearings were placed in all contact zones between shafts and supporting structure.



Figure 3.26 – Rollers and rack detail (CAD drawing).

In order to keep the weight low, these rollers were lathe machined based on a 10 mm aluminum circular rod. In Fig. 3.27, the final result of this structure can be seen.



Figure 3.27 – Actuation bay

## 3.6 System mass

After the construction work was complete, all components were weighed in order to evaluate the difference in mass between the conventional wing and telescopic wing. The resin used to impregna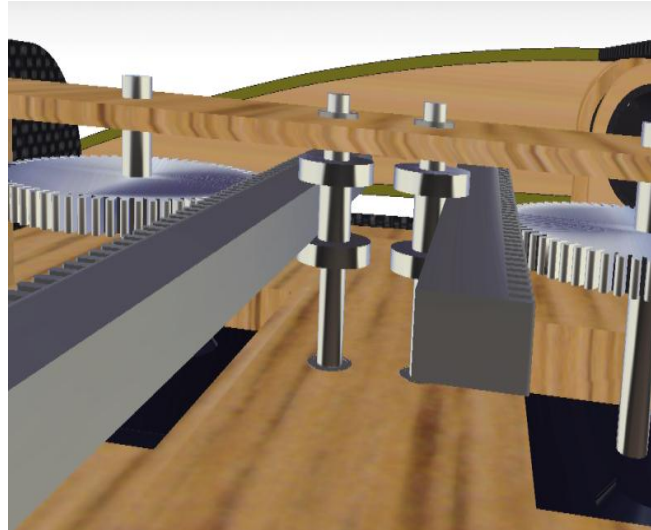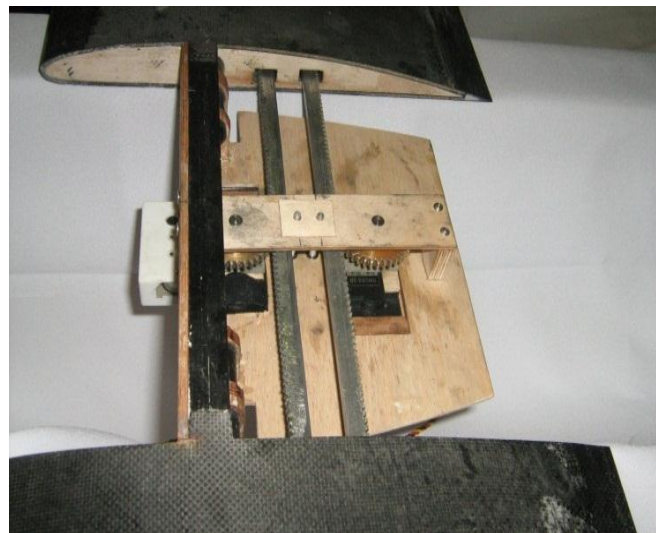te the composite skins is included in several weighed sets. A summary table is presented below with the total mass of the main components. Note that all ball bearings were not considered for the final mass. The wing's total mass, including the actuation mechanisms, is around 1.85 kg, as opposed to 1.3 kg of the originally wing developed for Olharapo UAV. This amounts to an increase of about 550 g which, is not too exaggerated given the difference in structural and actuation mechanism complexities that exist between the original wing and the telescopic wing.

| Part | Quantity | component | weight, g |
|---|---|---|---|
| OMW | 20 | Balsa ribs | 20 |
| | 2 | Carbon tubular spar | 108 |
| | 2 | Guide tube | 29 |
| | 2 | Skin | 142 |
| | 2 | Rack | 171 |
| | Total | OMW | 471 |
| IFW | 2 | Ribs | 25 |
| | 2 | Tensors | 115 |
| | 2 | Shells + foam | 570 |
| | Total | IFW | 852 |
| Actuation bay | 1 | board | 84 |
| | 2 | Modified Servo | 400 |
| | 1 | Fuselage linkages | 5 |
| | 4 | Board support | 8 |
| | 1 | Superior support | 9 |
| | 2 | Pinion | 90 |
| | Total | Actuation bay | 459 |
| | Total mass of VSW | | 1846 |
| Original Olharapo's wing mass | | | 1295 |

Table 3.2 – Summary of the final component weights and original Olharapo's Wing.

# Chapter 4

# VSW Evaluation and Results

A battery of tests was performed in order to evaluate the proper functioning of the system and determine the actual performance of the actuation system developed. Thus, two separate groups of tests were conducted: structural and the system actuator testing.

## 4.1 Structural Tests

### *Bending Test:*

This test, as the name implies, had as main objective of evaluating the strength and stiffness of the VSW. More specifically, the tip deflection of the wing was measured when it was subjected to different loads representing a range of flight load factors. The flight loads were simulated by placing sandbags on the telescopic wing's upper skin. For simplicity, the wing load distribution was considered constant in the fixed wing and triangular in the movable wing. Load factors were considered between $0g$ and $4.5g$. Also, all the sand bags were distributed along the main wing spar in order to avoid unnecessary torsion of the telescopic wing assembly. The tip deflection was determined by reading off a scale glued behind the wing tip. Figure 4.1 shows the assembly used to carry out the test.



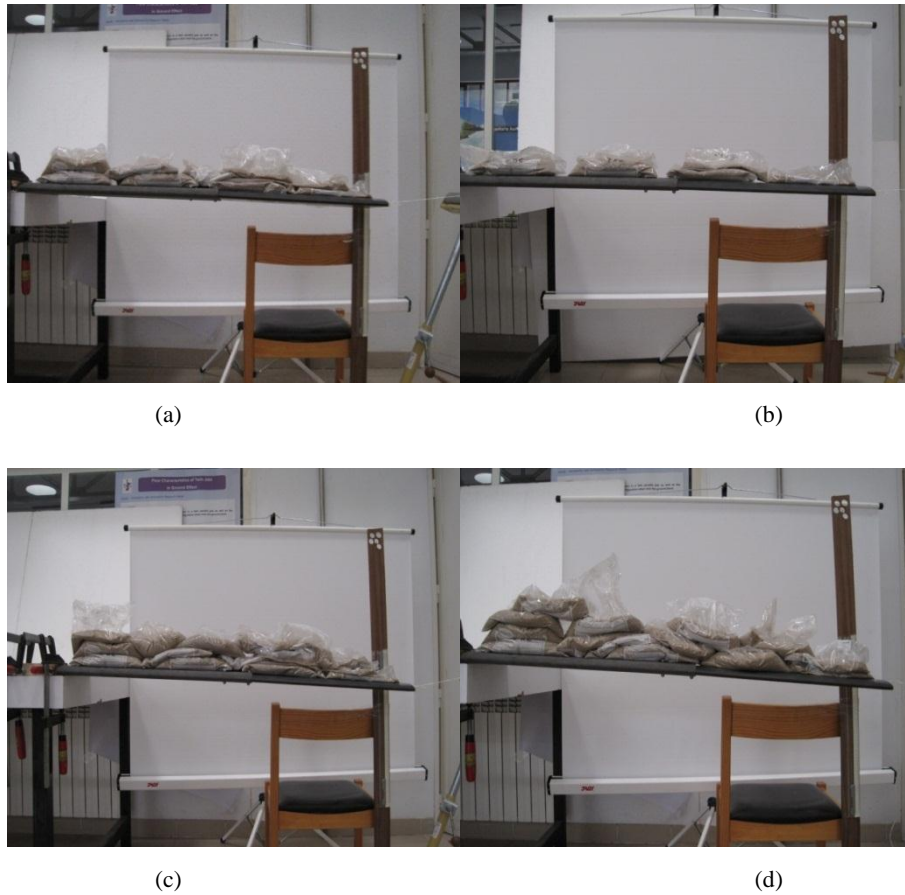Figure 4.1 – Assembly used for structural and system evaluation tests.

|                    |                    |
|:------------------:|:------------------:|
| (a)                | (b)                |
| (c)                | (d)                |

Figure 4.2 – Bending test: $1G - 3kgf$ (a), $2G - 6\ kgf$ (b), $3.5G - 10.5\ kgf$ (c) and $4.5G - 13.5\ kgf$ (d).

As can be observed from Fig. 4.2, the increase in load factor led to considerable increase in the wing tip vertical deflection. Also, a slight slope discontinuity was observed at the position where the movable wing enters the fixed wing, particularly at higher load factors. However, the OMW showed to be quite stiff, as it remained completely straight under load. Thus, the overlap of 100 mm between both wing parts resisted the bending loads by deforming the airfoil contour shape: effectively increasing the airfoil thickness. This localized bending was visible from the gap between the IFW upper skin and the OMW upper skin (Fig. X below). This gap became more apparent with higher load factor, reaching a value of about 2 mm under a $4.5g$ load.

Figure 4.3 – Gap between upper skins.

The following figure quantifies the variation in tip deflection with increasing load factor. It should be noted that for load factors of 3.5*g* and 4.5*g*, the tip deflection was about 40mm and 55mm, respectively, showing a good resistance to bending. The results were due, in part, to the lack of stiffness at the interface OMW and IFW interface. Improvements on this can easily be implemented in the future.
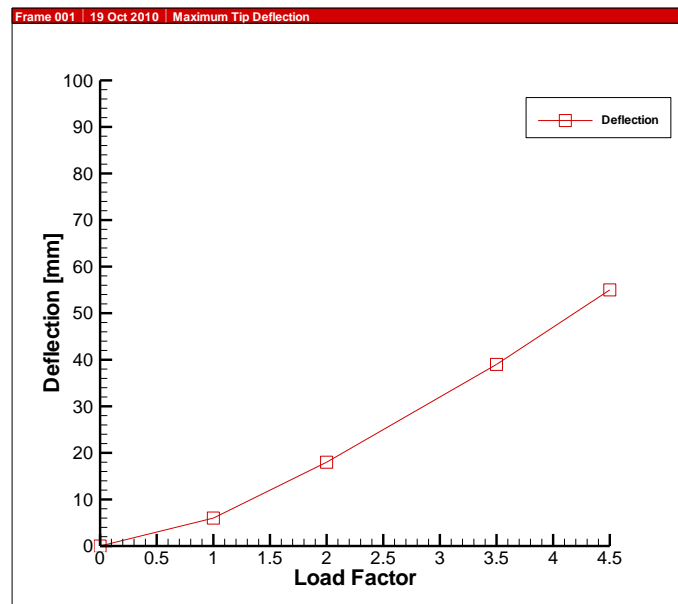


Figure 4.4 – Wing tip vertical deflection as a function of load factor.

## 4.2 Actuator system testing

## 4.2.1 Maximum actuation force test

The objective of the test was to measure the maximum force that the actuation mechanism could hold. To that end the assembly shown in Fig. 4.5 was used. In general, the rack was installed in the actuator, without the movable wing, a string was attached to its tip and supported by a roller that converts the horizontal movement into a vertical movement. At the end of the vertical part of the string weights with successively increased value were hung until the system actuator was no longer able to raise them.

Following that procedure, it was determined that the maximum weight lifted by the servo mechanism was 39.2N. The servo torque corresponding to this weight is $0,71\ N.m$, which is below the expected $0,93N.m$ as indicated by the servo manufacturer. This represents a value 24% lower than it was expected. Two distinct factors contributed to this result: the need for a high current intensity leading to a voltage drop supplied to the system and imperfections of the rack-pinion assembly (imperfections in the teeth were observed). The latter contributed to significant energy being lost that could otherwise be used to move the wing.



Figure 4.5 – Installation used in maximum actuation force test.

## 4.2.2 Extension/Retraction time test

Performed in the early stages, this tests led to the damage of the 5301 servos, which had to be replaced by the Hitech type. As a result, the deployment times were higher, still the comparison with or without ball bearings remains valid. For that reason, this test was not repeated.

This test aimed at measuring the telescopic wing's extension and retraction times for various load factors. At the same time the need for placing the ball bearings in the sandwich skin could be assessed. The approach used during the structural bending tests where weights were placed over the OMW was not appropriate in this case because this part of the wing was required to slide into the IFW during the actuation sequence. For this reason, instead of loading the OMW with the triangular load distribution an equivalent concentrated load was placed at the wing tip. The equivalent concentrated load was calculated so that the moment relative to the OMW and IFW interface was the same as that of the load distribution. Figure 4.6 illustrates the relationship between the load factor and the equivalent concentrated load at the tip of the wing.
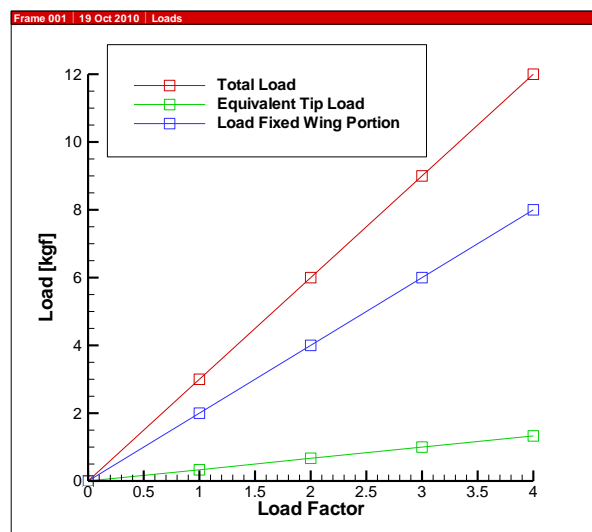


Figure 4.6 – IFW load, equivalent wing tip load and total load as function of load factor.

Full cycle times (extension followed by retraction) were measured using a digital stopwatch. This procedure leads to small errors due to operator reaction time. In future work it is suggested that the whole process is automated to avoid these errors.

Referring to Fig. 4.7, it is evident that the time of retraction/extension increased as load factor increased. This was already expected, since increasing the load factor increased friction between wing

parts and hence the servomotor had more difficulty in overcoming the increased force. Furthermore, the wing with the ball bearings produced slower retraction/extension times at lower load factors. However, for higher load factors, retraction/extension times of the wing with the ball bearings improved relative to the wing without the ball bearings. Based on these results it is premature to conclude that the bearings adversely affect the operation speed of the telescopic wing, since errors associated with the reaction time when using the stopwatch may have influenced the test.
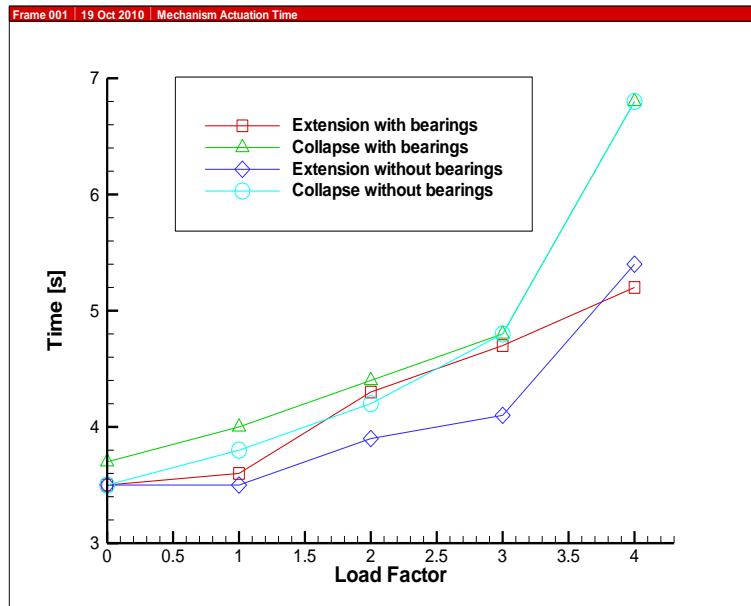


Figure 4.7 – Retraction and extension times for load factors, with and without ball bearings.

## 4.2.3 Power consumption and efficiency tests

To determine the mechanism efficiency, two separate measurements for various load factors ($0g$, $1g$, $2g$, $3g$ and $4g$) were performed. These were: (a) evaluating the energy entering the system, and (b) its useful work done.

As for the first test (a), an *e-logger* v3 form Eagle Tree Systems™ was used to determine the power consumed by the servo. This device made 10 readings per second and provided the maximum, minimum and average values over the selected period of time. For this test, a period of 30 seconds was established in order to minimize errors. Also, with the same purpose, and to ensure a point of comparison between the various load factors, an RC radio emitter Multiplex Royalevo 9 in "*test run*" mode was used. This mode sent a signal such that the servo would oscillate between the determined values for the desired time. Thus it was possible to eliminate human error in the process. After

mounting the system (Fig. 4.9), current and voltage values were obtained for various load factors (Fig 4.8).
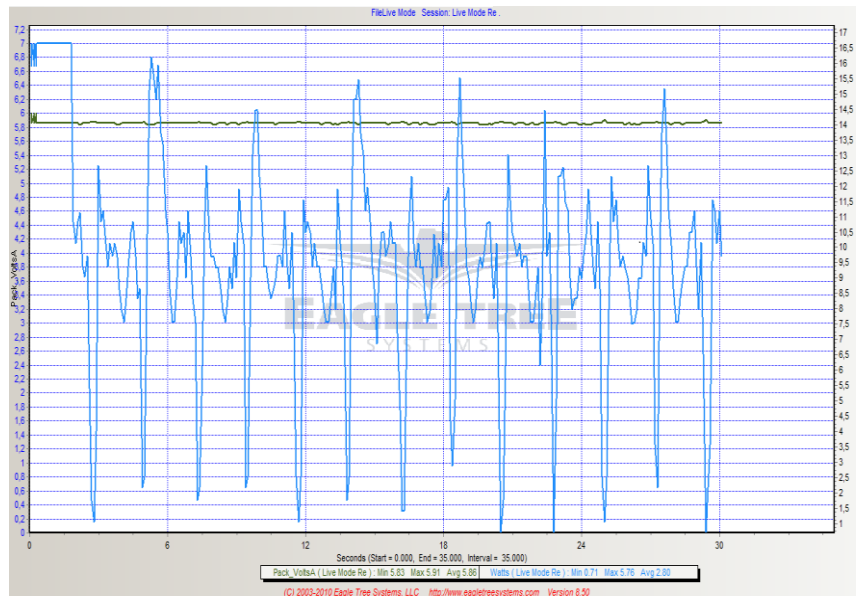


Figure 4.8 – example of the e-logger readings for the 4g case
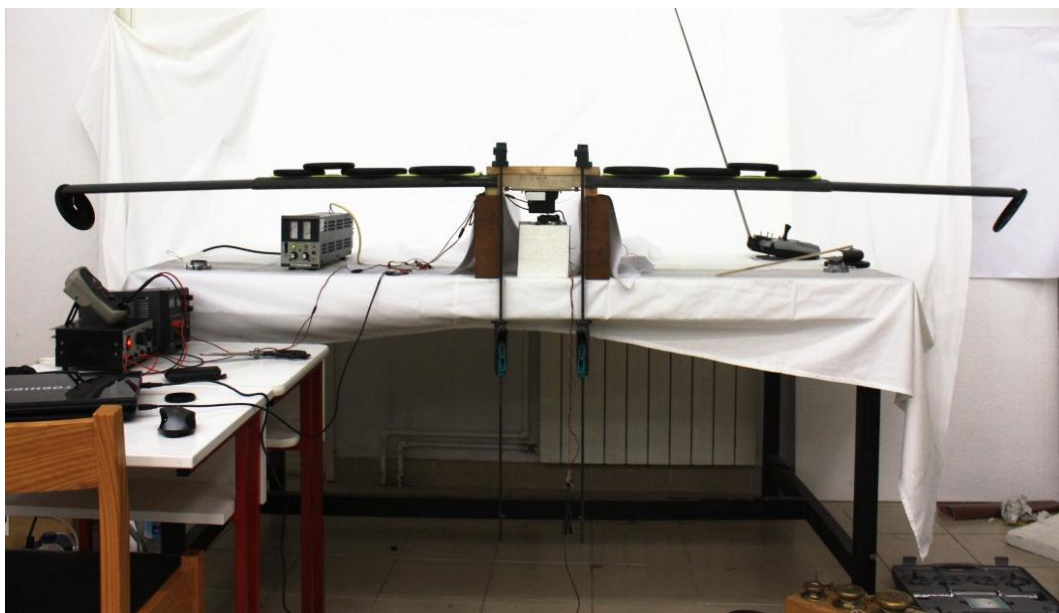


Figure 4.9 – Power consumption test assembly.

In the second test, in order to obtain the useful work, the average actuation force and the total deployment time was measured. At this point, several problems arose, since both tests, (a) and (b), had to be comparable. One of the suggested ideas to measure the mean actuation force laid on the use of a dynamometer to move the wing, though the value obtained would be the static friction and not the

average actuation force. Also, the addiction of sand bags was considered to measure the maximum force, though again presenting the same issue as the option above.

So, the best option was to use a load cell and register the voltage output level over time. Still, the problem of repetition of cycles used in test (a) remained. Having this in mind, one of the two servos was used to pull the load cell connected, on the other end, to the OMW. For a stable motion, the cell was mounted along a guide aligned with the VSW, ensuring a correct measurement of the force. The cell signal was registered by a *Picoscope2000* from pico technology and later converted into force through a program written in FORTRAN. After obtaining the force history, its average was easily calculated.
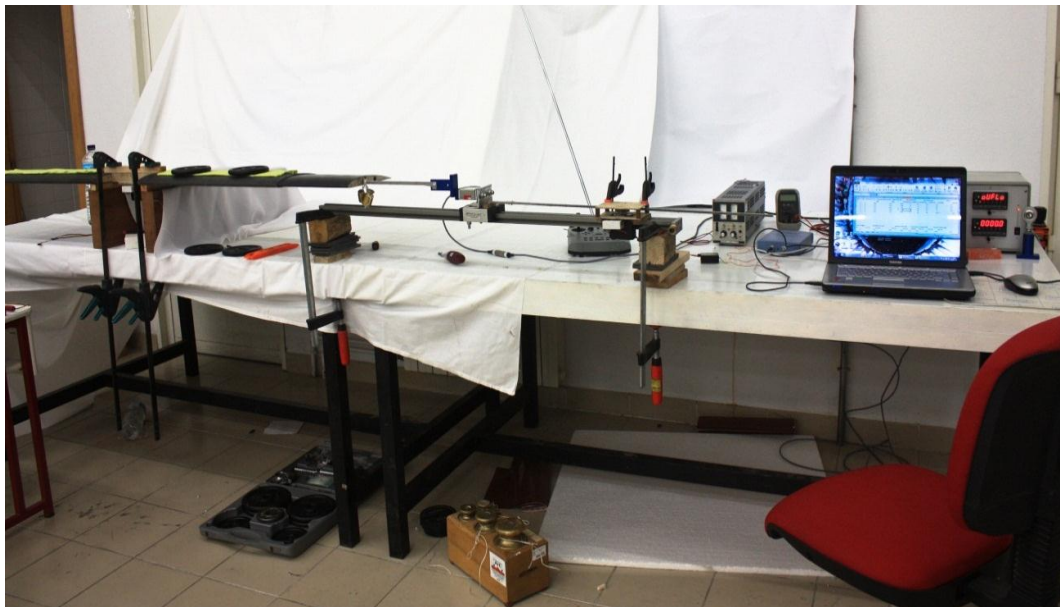


Figure 4.10 - Assembly to test the mean force.

During these experimental measurements, some peculiarities occurred that should be highlighted. Due to the servos' size, they absorb large amounts of current causing significant input voltage drops. These resulted in reductions in the available torque. This behavior was improved substantially by replacing the power cables with ones of higher cross-section area. As seen in Fig.4.8 the power consumption appear to be relatively stable. However, after carrying out the tests, voltage was measured at the leads of the servo with an oscilloscope and a high frequency voltage oscillation was found between 5 and 6 volts. The readings discrepancy was probably due to the e-logger's resolution, ten samples per second in this case. Having as its main function to measure the high consumption of electric motors, this application overcomes its ideal values. Figure 4.7 illustrates the force used to move the wing with a load factor of 4.
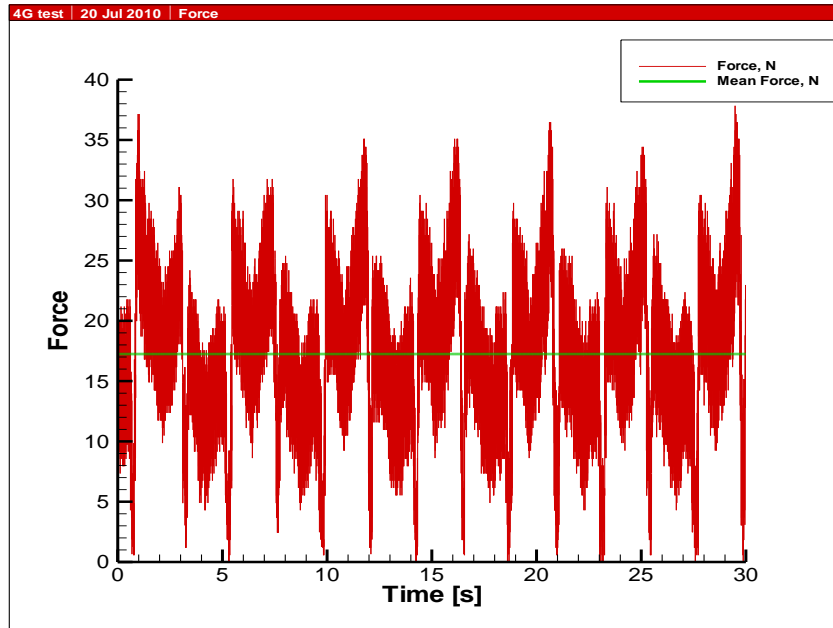
Figure 4.11 - graph of instantaneous and average force with a load factor of 4.

## *Calculations for the 4g load case:*

In order to exemplify the calculations used in this test, the 4*g* wing load case is described below. The total displacement is obtained through the multiplication of a single cycle displacement by 13 (number of total cycles).

$$F[N] \times d[m] = Work[J]$$

The result obtained is the useful work done by the servo to operate the VSW. The energy used is computed from the multiplication of the average power by the time during which it was applied:

$$Power[W] \times Times[s] = energy[J]$$

The efficiency of the mechanism can be obtained by the ratio between the energy provided and the useful work done.

These calculations were applied for every load factors. A summary of the various test results can be found in Table 4.3.

| Load Factor | Power [watt] | Time [s] | Energy [J] | Work [J] | Efficiency | Average Current [V] | Average Forçe [N] |
|---|---|---|---|---|---|---|---|
| 0 | 2.34 | 30 | 70.3 | 31.7 | 45% | 5.75 | 4.81 |
| 1 | 3.76 | 30 | 112.9 | 40.5 | 36% | 5.81 | 6.62 |
| 2 | 5.79 | 30 | 173.6 | 57.6 | 33% | 5.76 | 9.73 |
| 3 | 7.60 | 30 | 228.0 | 68.6 | 30% | 5.73 | 13.27 |
| 4 | 9.49 | 28 | 265.8 | 73.7 | 28% | 5.71 | 17.25 |

Table 4.1 – Consumption and efficiency test results.

In this table, it can be noted the expected increase in power consumption due to the higher wing loading and the consequent friction increase. It can be seen that, as load factor increases, the efficiency decreases. The explanation for that may be in the motor of the servo that reduces efficiency for higher currents and also the small construction imperfections that would become more harmful to the system when it starts to work with higher.

This test was devised to avoid human error. However, it could still be improved. One of the setbacks is justified by the assumption that the total displacement is the same in both tests (consumption and force tests), which was not necessarily true. Also, the voltage oscillation at the servo input should be addressed in future work.

# Chapter 5

# Summary

## 5.1 – Conclusions

This work led to important conclusions that are highlighted in this chapter.

The use of ball bearings in the upper and lower skins of the IFW proved to be detrimental to the sliding of the OMW. However, this modification could be complemented with two extra ball bearings placed at the trailing edge to prevent the excessive friction in that area. Because the structure is not stiff enough, if the upper and lower camber skins move further apart, the leading and trailing edges will approach, interfering with the OMW motion.

Bench tests were conducted to verify the real OMW deployment time. This test took into account various wing load factors and resulted in the values presented in Table 5.1. The time was measured with a digital clock, which could have led to small errors in the timing. In a future work, it is suggested that the whole process is automated to avoid these errors.

| Load Factor | 0 | 1 | 2 | 3 | 4 |
|---|---|---|---|---|---|
| Time [s] | 1.8 | 2 | 2.3 | 2.5 | 3 |

Table 5.1 – Time vs Load Factor

This deployment time leads us to believe that the aircraft can be roll controlled with this actuation system by asymmetrically deploying the wings.

The structural strength was proved in bench tests, showing that the wing can withstand loads up to $4.5g$ at its maximum wingspan value. The system efficiency was also evaluated. The result of the efficiency test was not as good as expected giving an efficiency of 43% for the $0g$ load case. Several factors may have contributed to this result: imperfections in construction, systems' gears and rack and

pinion set. This test aimed to determine a reference value, yet it can be improved in order to obtain more reliable results. This optimization can be achieved by automating, even more, mentioned test. Finally, this study allowed to develop and validate construction methods and identify critical processes and tasks in the manufacture and assembly of the final VSW prototype.

## 5.2 Future work

Similarly to other engineering works and projects, this one can always be improved and optimized, making the system even closer to the ideal. In this context, several areas can be considered for improvement.

As for structural issues, one of the most critical areas of this system is the interface zone between the OMW and the IFW. An effective solution that avoids contact between these two structures remains to be developed. As an option, a second set of ball bearings can be applied. To optimize the discontinuity zone, a way to fill the existing slack between OMW and IFW must be established. A solution may be the use of rubber rings ("Dust Rings") like those used in some damping systems. The OMW and IFW interface can be strengthened by introducing carbon fiber ribs replacing the PVC foam to avoid airfoil section deformation.

Still, some finite element simulations could be performed in order to identify and strengthen critical areas.

Control issues are of paramount importance in morphing technologies. The need to operate simultaneously more and more complex structures, modify and adapt them to all flight conditions and do it in useful time is a real and demanding problem. The solution relies not on the pilot, not on the human brain, but in the machine. To continue developing this work a span controller is needed to ensure a correct wing deployment at each flight condition. The retraction and extension of the wings must be performed automatically. This requires knowledge of flight speed and normal acceleration through sensors. A quick look at the roll control issue shows at least three possible situations to be considered to perform a steady turn from an initial cruise condition: at low speeds, with the wings fully deployed, one has to retract the inside-turn wing; at medium speeds, with the wings half deployed, one must retract the inside-turn wing and extend the outside turn wing (this can be performed proportionally or not); and at high speeds, with the wings fully retracted, one has to extend the outside-turn wing. Also, it is important to quantify the energy requirements to actuate this wing during a full typical mission and compare those with the original conventional wing with ailerons. By doing this it will be possible to assess whether the performance advantages of the variable span wing are not offset by power and weight requirements.

# Bibliography

[1] Blondeau, J., Richeson, J., and Pines, D. J., "Design, Development and Testing of a Morphing Aspect Ratio Wing Using an Inflatable Telescopic Spar", AIAA Paper 2003-1718, April 2003.

[2] Blondeau, J., and Pines, D. J., "Pneumatic Morphing Aspect Ratio Wing", AIAA Paper 2004-1808, April 2004.

[3] Blondeau, J., and Pines, D., "Design and Testing of a Pneumatic Telescopic Wing for Unmanned Aerial Vehicles", *Journal of Aircraft*, Vol. 44, No. 4, July-August 2007, pp. 1088-1099.

[4] Henry, J. J., Blondeau, J. E., and Pines, D. J., "Stability Analysis for UAVs with a Variable Aspect Ratio Wing", AIAA Paper 2005-2044, April 2005.

[10] Gamboa, P., Aleixo, P., Vale, J., Lau, F., and Suleman, A., "Design and Testing of a Morphing Wing for an Experimental UAV", The Applied Vehicle Technology Panel Symposium (AVT-146), Florence, Italy, 14-17 May, 2007.

[13] M. Czajkowski, G. Clausen, B. Sarh, "Telescopic wing of an advanced flying automobile", AIAA-1997-5602

[12] Mestrinho, J., Gamboa, P., "Projecto de Uma Asa Morphing de Envergadura Variável", Conferência Engenharia'2009 Inovação e Desenvolvimento, UBI, Covilhã, 25-27 Novembro, 2009.

[14] J. R.C. Mestrinho, J. M.I. Felício, P. D. Santos, P. V. Gamboa, "Design Optimization of a Variable-Span Morphing Wing", 2nd International conference on Engineering Optimization, Lisbon 6 – 9 September, 2010

[15] D. Cadogan, W. Graham, and T. Smith, "Inflatable and rigidizable wings for unmanned aerial vehicles". AIAA Paper 2003-6630, Sepember 2003.

[7] Cadogan, D., Scarborough, S., Gleeson, D., Dixit, A., Jacob, Dr. J., and Simpson, A., "Recent Development and Test of Inflatable Wings", AIAA Paper 2006-2139, May 2006.

[17] J. Jacob, S. Smith, R. Jones, S. Scarborough, and D. Cadogan. "A high-altitude test of inflatable wings for low-density flight applications". AIAA Paper 2006-1696, May 2006.

[19] L. Kheong and J. Jacob. "In flight aspect ratio morphing using inflatable wings". AIAA Paper 2008-425, January 2008.

[20] J. Bowman, B. Sanders, B. Cannon et al. "Development of Nex Generation Aircraft Morphing Structures". AIAA Paper 2007-1713

[21] G. Andersen, D. Cowan, D. Piatak. "Aeroelastic Modeling, Analysis, and testing of a Morphing wing Structure". AIAA Paper 2007-1734

[22] J. Flanagan, R. Strutzenberg, R. Myers et al. "Development and Flight Testing of a Morphing Aircraft, the NextGen MFX-1". AIAA Paper 2007-1707

[23] D. Neal, M. Good, C. Johnston et al. "Design and Wind-Tunnel Analysis of a Fully Adaptive Aircraft Configuration". AIAA Paper 2004-1727

[27] Ferdinand P. Beer, E. Russell Johnston, John T. Dewolf. *Mechanics of Materials*. McGraw-HILL, Third edition. 2001

[5] Bae, J., Seigler, T. M., and Inman, D. J., "Aerodynamic and Static Aeroelastic Characteristics of a Variable-Span Morphing Wing", *Journal of Aircraft*, Vol. 42, No. 2, March-April 2005, pp. 528-534.

[6] Bae, J., Seigler, T. M., Inman, D. J., and Lee, I., "Aerodynamic and Static Aeroelastic Considerations of A Variable-Span Morphing Wing", AIAA Paper 2004-1726, April 2004.

[8] Neal, D. A., Good, M. G., Johnston, C. O., Robertshaw, H. H., Mason, W. H., and Inman, D. J., "Design and Wind-Tunnel Analysis of a Fully Adaptive Aircraft Configuration", AIAA Paper 2004-1727, April 2004.

[9] Vale, J., Gamboa, P., Lau, F., and Suleman, A., "Optimization of a Morphing Wing Based on Coupled Aerodynamic and Structural Constraints", 3rd AIAA Multidisciplinary Design and Optimization Specialist Conference, Honolulu, Hawaii, USA, 23-26 April, 2007.

[11] Vale, J., Leite, A., Lau, F., and Suleman, A., "Design and Development of Strategies and Structures for Wing Morphing", RTO Applied Vehicle Technology Panel (AVT) Symposium, Évora, Portugal, 20-24 April, 2009.

[16] D. Cadogan, T. Smith, F. Uhelsky, and M. MacKusick. "Morphing inatable wing development for compact package unmanned aerial vehicles". AIAA Paper 2004-1807, 2004.

[18] J. Jacob, S. Smith, D. Cadogan, and S. Scarborough. "Expanding the small uav design space with inflatable wings". 07ATC-217, Society of Automotive Engineers Inc., 2007.

[24] EAGLE TREE SYSTEMS, LLC ™, URL http://www.eagletreesystems.com, June 2010

[25] Pico Technology, URL http://www.picotech.com/, June 2010

[26] Akademische Fliegergruppe im F.V.S, URL http://www.uni-stuttgart.de/akaflieg/-index.php?id=49&L=0&L=2, June 2010.